CD39^{+}PD-1^{+}CD8^{+} T cells mediate metastatic dormancy in breast cancer

Paulino Tallón de Lara[1,2,5,*], Héctor Castañón[1,2,*], Marijne Vermeer[1,2,**], Nicolás Núñez[1,2,**], Karina Silina[1,2], Bettina Sobottka[3], Joaquín Urdinez[4], Virginia Cecconi[1,2], Hideo Yagita[6], Farkhondeh Movahedian Attar[1,2], Stefanie Hiltbrunner[1,2,7] Isabelle Glarner[1,2], Holger Moch[3], Sònia Tugues[1,2], Burkhard Becher[1,2], Maries van den Broek[1,2,8]

[1]Institute of Experimental Immunology, University of Zurich, Zurich, Switzerland. [2]Comprehensive Cancer Center Zurich, Zurich, Switzerland. [3]Department of Pathology and Molecular Pathology, University Hospital Zurich, Switzerland. [4]Department of Orthopaedics, Balgrist University Hospital, University of Zurich Zurich, Switzerland. [5]Current address: Department of Medicine, Mount Sinai St. Luke's & Mount Sinai West, Icahn School of Medicine at Mount Sinai, New York, NY, USA. [6]Department of Immunology, Juntendo University School of Medicine, Tokyo, 113-8421, Japan. [7]Current address: Department of Hematology and Oncology, University Hospital Zurich, Zurich, Switzerland.

[8]Lead contact. Maries van den Broek, Institute of Experimental Immunology, University of Zurich, Winterthurerstrasse 190, 8057 Zurich, Switzerland. E-mail: vandenbroek@immunology.uzh.ch.

[*]Equal first-author contribution. [**]Equal second-author contribution.

Further information and requests for resources and reagents should be directed to and will be fulfilled by the Lead Contact Maries van den Broek (vandenbroek@immunology.uzh.ch).

Summary

Some breast tumors metastasize aggressively whereas others remain in a state of metastatic dormancy for months or even years. The mechanism governing such metastatic dormancy remains largely unknown. Through high-parametric single-cell mapping in mice, we identified a discrete population of $CD39^+PD\text{-}1^+CD8^+$ T cells present both in primary tumors and in dormant metastasis, which was hardly found in aggressively metastasizing tumors. Using blocking antibodies, we found that dormancy depended on TNFα and IFNγ. Of note, immunotherapy reduced the number of dormant cancer cells in the lungs. Adoptive transfer of purified $CD39^+PD\text{-}1^+CD8^+$ T cells prevented metastatic outgrowth. In human breast cancer, the frequency of $CD39^+PD\text{-}1^+CD8^+$ but not of total $CD8^+$ T cells correlated with delayed metastatic relapse after resection (disease-free survival), thus underlining the biological relevance of $CD39^+PD\text{-}1^+CD8^+$ T cells for controlling experimental and human breast cancer. Furthermore, density of $CD39^+PD\text{-}1^+CD8^+$ T cells may serve as a novel biomarker and may serve as a potential immunotherapy target. Thus, we discovered that a primary breast tumor primes a systemic, $CD39^+PD\text{-}1^+CD8^+$ T cell response that is essential for metastatic dormancy in the lungs.

Introduction

Metastasis is the major cause of death in patients with breast cancer. The metastatic behavior of this disease is heterogeneous regarding affected organs as well as timing[1,2]. Whereas some patients develop metastasis shortly after or even before diagnosis, others show metastatic lesions only years or decades after removal of the primary tumor[1,3]. In fact, approximately 20% of disease-free patients will relapse within 7 years after resection, and patients that appear to be cured from breast cancer have a higher mortality than the rest of the population even 20 years after surgery[4,5]. Such late relapses are thought to result from disseminated cancer cells (DCCs) that reached different organs but remained dormant for several years[6]. Indeed, the presence of DCCs in the bone marrow of breast cancer patients loosely correlates with the development of metastatic relapse[7,8].

The cancer cell-intrinsic and -extrinsic mechanisms governing metastatic dormancy are poorly understood. Some cancer cell-intrinsic factors have been associated with dormancy such as inhibition of the PI3K-AKT pathway[9], activation of p38 or triggering of an endoplasmic reticulum stress response[10]. In addition, the microenvironment in the (pre)metastatic organ may induce dormancy[11] by different signals such as an endothelial cell-derived thrombospondin-1[12] or TGF-β2 produced in the bone marrow[13]. Only few studies addressed the influence of cancer cell-extrinsic factors such as innate[14,15] and adaptive immunity[16,17] on dormancy. Although infiltration of the primary tumor by T cells was shown to correlate with a good prognosis[18], it

70 remains unclear whether this correlation is explained by cytotoxic T cells that
71 eliminate cancer cells or by T cells that prevent the outgrowth of cancer cells
72 and induce dormancy[19,20].
73 Here we sought to understand the mechanism that governs metastatic
74 dormancy of DCCs and discovered that the primary tumor primes a systemic,
75 $CD8^+$ T cell response that prevents metastatic outgrowth of DCCs in the lungs.
76 The protective T cells expressed markers that are generally associated with
77 activation and exhaustion. Promoting such a response may provide a rationale
78 for development of future immunotherapies that aim to prevent metastatic
79 relapse.
80
81 **Results**
82
83 *Disseminated 4T07 breast cancer cells are dormant*
84 We used two preclinical models for breast cancer that were originally derived
85 from the same spontaneous tumor in BALB/c mice, 4T1 and 4T07[21] (Figure
86 1A). 4T1 orthotopic breast cancer produces macro-metastasis in different
87 organs[22,23], whereas 4T07 is essentially non-metastatic. Some studies,
88 however, showed the presence of disseminated 4T07 cells in distal organs[21,24].
89 Orthotopically injected 4T1 and 4T07 cells showed comparable breast cancer
90 growth and incidence in immunocompetent BALB/c mice, although 4T1 tumors
91 grew faster at late stages (Supplemental Figures S1A and S1B). But, whereas
92 4T1 breast cancer readily induced aggressively growing and macroscopically
93 visible lung metastasis, 4T07 did not (Supplemental Figures S1C and S1D).

94 Despite absence of macro-metastasis, we found disseminated 4T07 cells in the
95 lungs (Supplemental Figure S1E) of all mice, suggesting that 4T07 DCCs seed
96 the lungs but fail to grow out. Presence of dormant DCCs in the lungs of all
97 mice bearing a 4T07-mCh primary tumor was confirmed and quantified by
98 immunofluorescence (Figures 1B, 1C and 1D, and Supplemental Figure S1F).
99 Disseminated 4T07 cells were present as single cells and were Ki67-negative,
100 as has been previously described for dormant DCCs[15,17]. The fact that we found
101 non-proliferating, disseminated 4T07 21 days after resection of the primary
102 tumor (Figures 1E and 1F) further underscores the dormant state of 4T07
103 DCCs.
104
105 *Breast cancer induces CD8$^+$ T cell-mediated immunity resulting in dormancy*
106 We first investigated whether cancer cell-intrinsic features influenced the
107 outgrowth of DCCs in the lungs by injecting 4T1 or 4T07 breast cancer cells
108 intravenously (i.v.) into naïve mice (Figure 2A). Under these experimental
109 conditions, both cell lines comparably formed macro-metastases (Figure 2B),
110 suggesting that both cell lines can progressively grow in the lungs.
111 The myeloid cell compartment was shown to undergo cancer-induced changes
112 that promote metastasis by creating a pre-metastatic niche in the 4T1
113 model[25,26]. Specifically, 4T1 primary tumors induce systemic neutrophilia[27] and
114 splenomegaly[26], as well as accumulation of inflammatory monocytes[28],
115 eosinophils, neutrophils[27] and alveolar macrophages[29] in the pre-metastatic
116 lung. We therefore compared 4T1- and 4T07-induced changes on the myeloid
117 compartment in blood and lungs and observed no differences regarding

118 splenomegaly (Supplemental Figure S2A), or neutrophilia (Supplemental
119 Figure S2B). The lungs of mice with 4T1 or 4T07 breast cancer were similar
120 concerning the presence of inflammatory monocytes (Supplemental Figure
121 S2C), neutrophils (Supplemental Figure S2D), eosinophils (Supplemental
122 Figure S2E) and alveolar macrophages (Supplemental Figure S2F) as
123 determined by flow cytometry (Supplemental Figure S2G). We saw the
124 previously reported accumulation of myeloid cells in the lungs during breast
125 cancer progression[27] in 4T1 and 4T07 alike (Supplemental Figure S2). Thus,
126 the difference in metastatic behavior of 4T1 and 4T07 breast cancer cannot be
127 explained by systemic changes in the myeloid compartment.
128 Orthotopic 4T07 tumors induced progressively growing lung metastases in T
129 cell-deficient BALB/c *Foxn1*$^{nu/nu}$ mice, whereas T cell-deficiency hardly
130 influenced metastatic behavior of 4T1 tumors (Figures 2C, 2D and 2E). To
131 compare lung metastases in both strains, we analyzed wild type and *Foxn1*$^{nu/nu}$
132 mice at the same time point after injection and added an additional group of
133 wild type mice in which breast tumors were allowed to progress until they
134 matched the size in *Foxn1*$^{nu/nu}$ mice (WT late) (Figures 2D and 2E). Thus,
135 metastatic dormancy of disseminated 4T07 breast cancer cells completely
136 depends on T cells. To study whether CD8^{+} T cells are responsible for
137 metastatic dormancy, we depleted CD8^{+} T cells from mice followed by
138 orthotopic injection of 4T07 cells and subsequent analysis of lung metastatic
139 load by IVIS (Figure 2F). While the growth of primary tumors was unaffected by
140 CD8-depletion, disseminated 4T07-LZ cells grew out to macro-metastases in

141 the absence of CD8+ T cells (Figures 2G and 2H), suggesting that primary 4T07
142 breast cancer induces CD8+ T cell-dependent immunity.
143 To test the hypothesis that CD8+ T cells are essential for metastatic dormancy,
144 we orthotopically injected untagged 4T07 cells (or PBS as control) followed by
145 an i.v. challenge with luciferase-tagged 4T07-LZ cells 11 days later (Figure 2I).
146 If the primary tumor had induced protective immunity, we would expect
147 metastatic dormancy of i.v. injected 4T07 cells in the lungs. Because we
148 measured lung metastatic load by bioluminescence, we specifically quantified
149 the i.v. injected, luciferase-tagged 4T07 cells. The presence of a primary 4T07
150 breast tumor prevented metastatic outgrowth of i.v. injected 4T07-LZ cells
151 (Figures 2I, 2J and 2K) but did not influence the amount of seeding as
152 measured 0.5 and 3 h after i.v. injection (Supplemental Figures S3A and S3B).
153 At the endpoint, i.v. injected cells were present as disseminated, non-cycling
154 single 4T07 cells in the lungs (Supplemental Figures S3C and S3D). Resection
155 of the primary tumor before i.v. challenge did not interfere with dormancy.
156 Specifically, i.v. injected 4T07-mCh cells readily induced macroscopically
157 visible lung metastasis in control mice (PBS in breast and mock surgery;
158 Supplemental Figures S3E and S3F), whereas only single, non-proliferating
159 4T07 cells were detected in the lungs of 4T07 tumor-bearing mice, independent
160 of resection (Supplemental Figures S3E and S3G). We confirmed these results
161 in a similar experimental set-up using 4T07-LZ cells and bioluminescence as
162 read out (Supplemental Figures S3H and S3I). Depletion of CD8+ cells before
163 i.v. challenge enabled metastatic outgrowth (Figures 2L and 2M), confirming
164 the dependence of dormancy on CD8+ T cells. In contrast, 4T07 nor 4T1 breast

165 cancer protected against experimental 4T1 lung metastasis, although 4T07-
166 induced systemic immunity reduced the metastatic load resulting from i.v.
167 injected 4T1-LZ cells (Supplemental Figures S3J and S3K).
168 Together, these data suggest that 4T07 breast cancer induces a systemic,
169 protective immune response that mediates dormancy of DCCs in the lungs.
170
171 *CD39$^+$PD-1$^+$CD8$^+$ T cells mediate metastatic dormancy*
172 Since we found that 4T07 metastatic dormancy depends on CD8$^+$ T cells, we
173 characterized these cells in 4T1 and 4T07 primary tumors by high-dimensional
174 flow cytometry. First, we gated on T cells (Supplemental Figure S4A), visualized
175 all the markers in our 23-parameter panel using a two-dimensional *t*-stochastic
176 neighbor embedding (tSNE) projection[30] (Figure 3A) and clustered the cells
177 using FlowSOM[31,32] (Figures 3A and 3B, upper panels and lower left panel).
178 Based on the median marker intensities observed in the clusters (Figure 3B,
179 lower right panel), we annotated the major T cell populations (CD8$^+$ T cells,
180 CD4$^+$ T cells, and CD4$^+$ CD25$^+$ regulatory T cells) and determined their
181 frequency and the position of each population in the tSNE projection. 4T07
182 primary tumors contained a higher proportion of CD8$^+$ T cells (Figure 3B, lower
183 left panel). We identified a discrete population of CD39$^+$PD-1$^+$CD8$^+$ T cells
184 present both in primary 4T07 tumors and in dormant metastasis, which was
185 hardly found in aggressively metastasizing 4T1 tumors. The frequency of
186 regulatory T cells was similar in 4T1 and 4T07 tumors, while conventional CD4$^+$
187 cells were more abundant in 4T1 tumors compared to 4T07. Of note, within the

188 CD8 compartment (Figure 3C), we observed that 4T07 breast cancer
189 accumulated CD39^{+}PD-1^{+}CD8^{+} T cells (Figure 3D).
190 To substantiate that enrichment of CD39^{+}PD-1^{+}CD8^{+} T cells is the key
191 immunological difference between 4T07 and 4T1 breast cancers, we analyzed
192 our high-dimensional flow cytometry data using the unbiased representation-
193 learning algorithm CellCnn[33,34]. In agreement with FlowSOM analysis, CellCnn
194 detected a population with high expression of CD39, PD-1, LAG3 and Tim-3
195 (Figure 3E and Supplemental Figure S4B). Indeed, the two markers that best
196 defined the population and showed the biggest differential abundance in terms
197 of the Kolmogorov–Smirnov two-sample test between the whole-cell population
198 and the selected cell subsets (higher KS value) were PD-1 and CD39 (Figure
199 3E). This population was around 3 times more abundant in 4T07 compared to
200 4T1 tumors (Figure 3H, $p<0.001$).
201 In addition, CD39^{+}PD-1^{+}CD8^{+} T cells expressed more of LAG-3 and Tim-3
202 (Figure 3F), which characterizes this population as effector cells that
203 experienced recent T cell receptor engagement[35,36] but may also indicate
204 exhaustion[37,38]. Therefore, we analyzed the functionality of CD39^{+}PD-1^{+}CD8^{+}
205 T cells sorted from 4T07 tumors and confirmed the production of IFNγ and
206 TNFα (Supplemental Figure S4C), suggesting that CD39^{+}PD-1^{+}CD8^{+} T cells in
207 4T07 tumors possess protective effector functions.
208 Importantly, CD39^{+}PD-1^{+}CD8^{+} T cells are found in the lungs of mice with
209 primary 4T07 breast cancer (Figure 3I). A proportion of this population
210 expresses CD103, hence resembling tissue-resident memory T cells[39,40]
211 (Figure 3J). Our observation that CD39^{+}PD-1^{+}CD8^{+} T cells didn't express

212 CD103 in the primary tumor (Figure 3F) is in line with recent data showing that
213 tissue-resident-like memory cells in human breast cancer are CD103-
214 negative[41]. Thus, accumulation of CD39$^+$PD-1$^+$CD8$^+$ T cells is the main
215 immunological difference between dormant and metastatic tumors.
216 Because the CD8$^+$ cells specifically emerging in 4T07 express PD-1, we
217 wondered whether blocking PD-1 may improve their presumed protective
218 effect. Indeed, immunotherapy with anti-PD-1 reduce the number of
219 disseminated 4T07 cells in the lungs approximately twofold (Figures 4A and
220 4B), suggesting that the PD-1$^+$ subset of CD8$^+$ T cells comprises protective
221 effector cells. To investigate whether the CD39$^+$PD-1$^+$CD8$^+$ T cell subset
222 indeed controls metastatic outgrowth and therefore mediates metastatic
223 dormancy, we sorted this population from 4T07 breast cancer and adoptively
224 transferred them to naïve BALB/c mice followed by an i.v. injection of 4T07-LZ
225 cells (Figures 4C and 4D). Adoptive transfer of CD39$^+$PD-1$^+$CD8$^+$ T cells
226 prevented 4T07 lung metastasis, whereas injection of PBS or CD8$^+$ T cells
227 lacking CD39$^+$PD-1$^+$ cells (referred to as other CD8$^+$ T cells) did not (Figures
228 4E and 4F). Thus, our results suggest that CD39$^+$PD-1$^+$CD8$^+$ T cells control
229 disseminated 4T07 breast cancer cells.
230 The presence of non-proliferating disseminated 4T07 cells in the lungs
231 suggests that CD8$^+$ T cells mediate dormancy by cell cycle arrest. Therefore,
232 we tested whether CD39$^+$PD-1$^+$CD8$^+$ T cell-derived IFNγ and TNFα can induce
233 senescence[42] by exposing 4T07 cells to those cytokines in vitro. We observed
234 a significant increase in the number of senescent cells as measured by
235 expression of senescence-associated β-galactosidase activity (Supplemental

236 Figures S5A and S5B). To confirm the relevance of IFNγ/TNFα-induced
237 senescence induction in vivo, we blocked both cytokines in mice with 4T07-
238 mCh breast cancer and analyzed the status of disseminated 4T07 cells in the
239 lungs by immunofluorescence (Figure 4G). Blocking IFNγ plus TNFα allowed
240 the outgrowth of disseminated cells as illustrated by the presence of clusters of
241 proliferating 4T07 cells (Figure 4H).
242 Thus, 4T07 primary tumors prime systemic CD8$^+$ T cells that induce cell cycle
243 arrest of DCCs by IFNγ and TNFα and thereby prevent overt metastatic
244 disease.
245
246 *CD39$^+$PD-1$^+$CD8$^+$ T cells have a transcriptome rich in effector and exhaustion*
247 *molecules*
248 To understand why this population controls DCCs, we sorted CD39$^+$PD-1$^+$CD8$^+$
249 and other CD8$^+$ T cells from 4T07 breast cancer and compared their
250 transcriptome (Figures 5A and 5B and Supplemental Figure S6A). CD39$^+$PD-
251 1$^+$CD8$^+$ cells show overrepresentation of transcripts associated with effector
252 function including *Prf1, Fasl, Gzmf, Gzme, Gzmd, Gzmc, Gzmb, Gzmk and Ifng*
253 (Figure 5C). This was confirmed by gene set enrichment analysis (GSEA)[43]
254 showing that the transcriptome of the sorted CD39$^+$PD-1$^+$CD8$^+$ cells shows
255 strong similarities with human tissue-resident CD8$^+$ T cells (Figure 5D), which
256 were recently shown to correlate with improved survival in triple negative breast
257 cancer[19]. This is in line with their unique capacity cells to prevent metastatic
258 progression. Furthermore, the fact that dormancy is never observed in 4T1
259 breast cancer is explained by the low number of such protective T cells in 4T1-

260 bearing hosts (Figure 3) and not by their transcriptional signature, since
261 CD39+PD-1+CD8+ cells from 4T1 and 4T07 tumors did not show many
262 differences (Supplemental Figures S6B, S6C and S6D). The transcriptome of
263 CD39+PD-1+CD8+ cells was also enriched in markers of activation and
264 exhaustion such as *Vsir* (VISTA), *Tnfrsf18* (GITR), *Tigit*, *Cd224* (2B4), *Tnfrsf9*
265 (4-1BB), *Tnfrsf4* (OX-40), *Icos*, *Lag-3*, *Ctla4* and *Havcr2* (Tim-3). This is
266 consistent with their overexpression of the transcription factor TOX (Figure 5C)
267 which leads to expression of exhaustion markers and persistence of effector
268 function during chronic antigen stimulation[44].
269 Taken together, CD39+PD-1+CD8+ cells have a unique transcriptomic signature
270 defined by the co-expression of immune checkpoint molecules and effector
271 proteins.
272
273 *CD39+PD-1+CD8+ but not total CD8+ T cells correlate with increased disease-*
274 *free after resection survival in breast cancer patients*
275 To investigate the clinical relevance of our preclinical findings, we analyzed
276 primary breast cancer tissues from a cohort of 54 patients, who had a
277 metastatic relapse after primary tumor resection (Table 1) for the presence of
278 CD8, CD39, PD-1 and epithelial cells using 5-plex immunofluorescence (Figure
279 6A). Our cohort shows the typical survival curves for the individual subtypes,
280 suggesting that it is representative (Supplemental Figure S7A). Patients with a
281 high density of intra-tumoral CD39+PD-1+CD8+ T cells had a significantly longer
282 disease-free survival after surgery than patients with a low density of such cells
283 (Figure 6B). The density of extra-tumoral CD39+PD-1+CD8+ T cells did not

284 correlate with disease-free survival (Supplemental Figure S7B), whereas to
285 density of CD39$^+$PD-1$^+$CD8$^+$ T cells independent of their location did
286 (Supplemental Figure S7C). In addition, we observed similar data when
287 focusing on luminal A and B patients (Supplemental Figures S7D and S7E).
288 The density of intra-tumoral CD39$^+$PD-1$^+$CD8$^+$ T cells was not an independent
289 variable according to multivariate Cox regression analysis (Table 1).
290 Importantly, the density of intra-tumoral CD8$^+$ T cells showed no correlation with
291 disease-free survival (Figure 6C), strongly supporting our preclinical
292 observations, namely that that disseminated cancer cells are controlled by this
293 specific subset of CD39$^+$PD-1$^+$CD8$^+$ T cells.
294
295 **Discussion**
296
297 We discovered that breast cancer can prime a systemic, CD8$^+$ T cell response
298 that mediates metastatic dormancy in the lungs and consequently, protects
299 against clinical metastatic outgrowth. We thus describe an unexpected trait of
300 primary tumors, in addition to their well-known metastasis-promoting
301 capacity[25,26,45,46]. Using high-dimensional single-cell profiling of primary tumors,
302 we identified the protective CD8$^+$ T cell population as PD-1$^+$ and CD39$^+$ cells,
303 suggesting recent cognate interaction and tumor-specificity[20,47]. In line with our
304 preclinical data, we found that a high density of intra-tumoral CD39$^+$PD-1$^+$CD8$^+$
305 T cells significantly correlated with disease-free survival after resection in breast
306 cancer patients. Even in patients with luminal A or B subtypes, where the tumor
307 tissue is generally less infiltrated by CD8$^+$ T cells[48], the presence of CD39$^+$PD-

308 1^{+}CD8^{+} T cells correlated with disease-free survival after primary tumor
309 resection. As in our preclinical model, the heterogeneous population containing
310 all CD8^{+} T cells did not correlate with disease-free survival, strongly supporting
311 the notion that CD39^{+}PD-1^{+}CD8^{+} T cells comprise a population of cells that is
312 uniquely equipped to control disseminated cancer cells.
313 The role of CD39 in cancer is rather complex. On the one hand, there is
314 evidence that CD39 expression marks tumor-specific T-cells and presence of
315 such cells correlates with a better prognosis or immune-mediated control[47]. On
316 the other hand, CD39 is constitutively expressed by some cancer cells and
317 suppressive cell types in the tumor microenvironment (Tregs and myeloid cells)
318 and catalyzes pro-inflammatory extracellular ATP (eATP), resulting in impaired
319 CD8^{+} T cell-dependent tumor control[49,50]. The same papers described a
320 reduction in tumor-associated macrophages and monocytes as well as a better
321 T cell function (and tumor control) after blocking the enzymatic activity of CD39.
322 We observed that CD39^{+}PD-1^{+}CD8^{+} T cells express effector molecules but also
323 markers that are typically associated with exhaustion. A similar population was
324 recently described in human breast cancer[19,51–53]. Exhausted T cells are
325 thought to have a reduced effector function and loss of proliferative
326 capacity[54,55]. Nonetheless, exhausted T cells in breast cancer may be more
327 functional than in melanoma[56].
328 In addition to local immunity, the induction of systemic immune responses by
329 immunotherapy was shown to be essential for its efficacy[57], suggesting that
330 protective CD8^{+} T cells are recruited to the tumor. Recirculating CD8^{+} T cells
331 can also enter tissues, where they develop into CD103^{+} tissue-resident memory

332 cells and may protect tissues against disseminating tumor cells by the induction
333 of cell death or cell cycle arrest[58]. Indeed, we detected $CD39^+PD\text{-}1^+CD8^+$ T
334 cells in the primary tumor and in the lungs and found that a proportion
335 expressed CD103 as a marker of tissue residency. It was recently shown that
336 the presence of intra-tumoral CD103-expressing $CD8^+$ T cells correlate with
337 survival in human breast cancer[41].
338 As mentioned above, metastatic dormancy may result from two different
339 states[59]: Disseminated single cells that are quiescent[60], or micro-metastases
340 that remain stable through an equilibrium between proliferation and death[61]. We
341 found that disseminated 4T07 cells were present in the lungs as single non-
342 cycling cells, suggesting dormancy through cell cycle arrest. Our observation
343 that dormancy essentially depended on $CD8^+$ T cells uncovers a novel
344 mechanism underlying dormancy. We found that protective $CD39^+PD\text{-}1^+CD8^+$
345 T cells produced TNFα and IFNγ, which were described to induce irreversible
346 senescence in the context of Th1-mediated protection against cancer[42]; the
347 same cytokines prevented proliferation of disseminated 4T07 breast cancer
348 cells in the lungs.
349 It may be that environmental cues induce cancer stem cell-like properties in
350 disseminated cancer cells[62], which is in line with the low cycling frequency.
351 Such cancer stem cells would represent a potent reservoir for progressive
352 metastasis[63] in response to environmental changes. Why dormant cancer cells
353 sometimes awaken only after decades[3] is still enigmatic, and it cannot be
354 excluded that different pathways converge to initiate growth of dormant lesions.
355 Assuming $CD8^+$ T cells are required for maintenance of dormancy it is

356 conceivable that attrition of tissue-resident memory CD8+ T cells may result in
357 awakening of dormant cells. Tumor resection and consequent loss of antigen
358 may result in diminished immunological memory; tissue-resident memory cells
359 are described to be particularly unstable in the absence of antigen[64,65].
360 Alternatively, dormant cells themselves may change, for example losing the
361 expression of molecules preventing immune-mediated clearance[66]. Finally,
362 environmental factors in the broadest sense may awaken dormant cancer cells.
363 Such changes in the microenvironment include fibrosis[67], tissue remodeling[68],
364 obesity[69], inflammation[70], disturbance of vascular homeostasis[71],
365 glucocorticoids[72], or cigarette smoke[73]. How such factors induce cycling of
366 dormant cells and whether immune cells can interfere at this stage is unknown.
367 Here we discovered that CD39+PD-1+CD8+ T cells mediate dormancy of
368 disseminated cancer cells but are by themselves unable to fully eradicate all of
369 the cancer cells. This is clinically highly relevant, as dormant cancer cells are
370 in all likelihood the source of future metastatic disease. Because the factors
371 determining awakening are not known and may even not be controllable, it is
372 important to better understand the nature of dormant cancer cells and which
373 pathways must be mobilized for their complete elimination.
374
375 **Acknowledgments**
376
377 We thank Anne Müller, Lubor Borsig and Christian Münz (all University of
378 Zurich) for valuable input and support. We thank Fred Miller (Karmanos Cancer
379 Institute) for providing cell lines. We thank the personnel from the Zurich

Integrative Rodent Physiology (ZIRP, University of Zurich) and the Laboratory Animal Services Center (LASC, University of Zurich) for expert animal care. We thank Ruben Casanova (University of Zurich) for developing the R script converting immunofluorescence image data into file format compatible with flow cytometry data analysis software. This work was financially supported by the Swiss National Science Foundation (SNSF; CRSII5_177208 and 310030_175565 (MvdB), as well as 310030_170320, 310030_188450 and CRSII5_183478 (BB)), the Swiss Cancer League (Oncosuisse; KLS-4098-02-2017 (MvdB) and KFS-4431-02-2018 (BB)), the University of Zurich Forschungskredit (PTdL and HC), the University Research Priority Program (URPP) Translational Cancer Research (MvdB, BB), the Science Foundation for Oncology (SFO; (MvdB)), the Helmut-Horten Foundation (MvdB), the Hartmann-Müller Foundation Zurich (MvdB), the Monique-Dornonville-de-la-Cour Foundation Zurich (MvdB) and the European Union H2020 Project iPC #826121 (BB).

Author contributions

PTdL, HC and MvdB conceived experiments; PTdL, HC, MV, NN, PC, EMC, VC, KS, FMA, JU, IG, MPL, SH performed and analyzed experiments; PTdL, HC, BB and MvdB wrote the manuscript; BB, ST, BS, HY and HM provided essential reagents; BB helped with data analysis; PTdL, HC and MvdB secured funding.

405 **Declaration of interests**

406

407 The authors declare no conflicting interests.

408 **Methods**

409

410 *Mice*

411 BALB/cJRj and BALB/cAnNRj-*Foxn1*$^{nu/nu}$ were purchased from Janvier labs
412 (Roubaix, FR). NOD.Cg-*Prkdc*^{scid}*Il2rg*^{tm1Wjl}/SzJ mice were originally obtained
413 from the Jackson Laboratory and provided by Christian Münz (University of
414 Zurich, Switzerland). Mice were kept under specific pathogen-free conditions in
415 individually ventilated cages at the Laboratory Animal Services Center at the
416 University of Zurich. Mice had access to food and water *ad libitum* and were
417 maintained on a 12-hour light/dark cycle with environmental enrichment. All
418 experiments were performed with 8-14-weeks-old female mice in accordance
419 with the Swiss federal and cantonal regulations on animal protection and were
420 approved by The Cantonal Veterinary Office Zurich (156/2018).

421

422 *Cell lines*

423 4T07 and 4T1 cells were a gift from Fred Miller (Karmanos Cancer Institute,
424 Detroit, USA). Cells were cultured in Dulbecco's Modified Eagle's Medium
425 (DMEM, Gibco) supplemented with 10% fetal bovine serum (FBS,
426 ThermoFisher Scientific), 2 mM L-glutamine and 2% penicillin/streptomycin
427 (ThermoFisher Scientific). Cells were cultured at 37°C in a humidified
428 atmosphere with 5% CO_2. 4T1 and 4T07 were lentivirally transduced to express
429 firefly luciferase and ZsGreen (pHIV-Luc-ZsGreen, addgene plasmid #39196)
430 or mCherry (pCDH-CMV-mCherry-T2A-Puro, addgene plasmid #72264).

431 Transduced cells were sorted based on expression of GFP or mCherry,
432 respectively. Luciferase-ZsGreen is referred to as LZ, mCherry as mCh.
433 Only cells of early passages were used for experiments. Cells were regularly
434 tested negative for mycoplasma by PCR analysis. Cells were also tested
435 negative for 18 additional mouse pathogens by PCR (IMPACT II Test, IDEXX
436 Bioanalytics).
437
438 *In vivo tumor experiments and treatments*
439 Hundred-thousand 4T1 or 4T07 cells in 50 μl PBS were injected into the fourth
440 mammary fat pad. Alternatively, 3 x 10^5 cells in 50 μl PBS were injected into
441 the lateral tail vein.
442 For resection of primary tumors, mice were anesthetized with 2.5 % isoflurane
443 and given 0.04 mg/kg fentanyl (Kantonsapotheke Zurich) i.p. as pre-emptive
444 analgesia. Primary tumors were resected, and wounds were closed using
445 Autoclip wound clips (BD Biosciences). For post-operative analgesia 0.1 mg/kg
446 buprenorphine (Temgesic, Schering-Plough) was given i.p. immediately after
447 surgery and in the drinking water at 10 μg/ml for 48 hours ad libitum.
448 For depletion of $CD8^+$ T cells, 500 μg rat anti-mouse CD8 (clone YTS 169.4,
449 hybridoma originally obtained from H. Waldmann, Oxford, United Kingdom)
450 was injected intraperitoneally (i.p.) in PBS as described in each experiment.
451 Control mice were injected with 500 μg rat anti-Trinitrophenol (clone 2A3,
452 BioXCell). Antibodies were purified from hybridoma culture supernatant using
453 protein G Sepharose 4 Fast Flow (Sigma). Injection of the respective antibody
454 resulted in depletion of >90% of $CD4^+$ or $CD8^+$ T cells for at least 14 days, as

455 determined by flow cytometry. Antibodies were administered i.p. in 200 μl PBS.
456 Full depletion of the targeted population was confirmed by flow cytometry on
457 blood 2 d after injection of the antibody in every experiment.
458 For blockade of PD-1, mice were injected with 250 μg anti-PD-1 (clone RMP1-
459 14, made in-house by H. Yagita) as indicated. Control mice received 250 μg
460 rat-anti-trinitrophenol (clone 2A3, BioXCell).
461 For blockade of INFγ and TNFα, mice were injected every 3rd day starting on
462 day 3 until the endpoint with 500 μg anti-INFγ (clone R4-6A2, BioXCell) plus
463 500 μg anti-TNFα (clone XT3.11, BioXCell) in 150 μl PBS. Control mice
464 received 1000 μg rat-anti-trinitrophenol (clone 2A3, BioXCell).
465 Lung metastasis from luciferase- or mCherry-expressing tumors was quantified
466 using an IVIS200 imaging system (PerkinElmer) as previously described[23].
467 Briefly, for luciferase-expressing tumors, mice were injected i.p. with 150 mg/kg
468 D-luciferin (Promega) and photon flux was measured 20 minutes later in vivo
469 as well as from dissected lungs. Lung metastasis from parental tumors was
470 quantified by India Ink as previously described[23]. Briefly, mice were euthanized
471 and India Ink (Pelikan, 15% in PBS) was injected intratracheally, lungs were
472 harvested, washed in PBS and fixed in Fekete's solution (62% ethanol, 3.3%
473 formaldehyde, 0.25 M acetic acid). Metastatic foci were counted blinded using
474 a dissection microscope.
475 Disseminated cancer cells were detected in the lungs using a colony forming
476 assay as previously described[21]. Briefly, lungs were resected from euthanized
477 mice, cut into small pieces and digested for 45 minutes at 37°C in DMEM with
478 1 mg/ml collagenase IV and 2.6 μg/ml DNase I (both Sigma) on a rotating

479 device. Subsequently, samples were washed with PBS by centrifugation at 350
480 *g*. For detection of circulating cancer cells, blood was collected by heart
481 puncture in a 25-gauge syringe containing 100 µl heparin (5'000 IU/ml, Braun)
482 and cells were washed with PBS by centrifugation at 350 *g*. Blood and lung
483 samples were suspended in complete DMEM containing 6 *µ*M of 6-thioguanine
484 and cultured in a T175 flask. Medium was exchanged after 5-7 days and
485 presence of colonies of tumor cells was evaluated after 14 days by light
486 microscopy and crystal violet staining.
487
488 *Immunofluorescence of mouse samples*
489 Organs were fixed with 4% paraformaldehyde (Roti-Histofix 4%, Roth) for 10
490 minutes at RT and cryoembedded in Optimal Cutting Temperature (O.C.T.)
491 Compound (O.C.T.™ Compound, Tissue-Tek) using dry ice/100% ethanol
492 slurry. Ten-*µ*m thick sections cut using a cryotome (Leica), mounted on
493 SuperFrost glass slides, dried for 1h at 37°C and preserved at -80°C until
494 immunostained. To prevent unspecific binding of antibodies, slides were
495 incubated with 4% donkey serum in PBS (ANAWA BioWorld) for 10 minutes at
496 RT. Subsequently, slides were incubated overnight at 4°C with primary
497 antibody diluted in PBS 1% donkey serum. Following primary antibodies were
498 used: Anti-mCherry (goat polyclonal antibody, AB8181-200 SICGEN, 1:400),
499 Ki67 (rabbit monoclonal antibody, ab16667 abcam, 1:100). After incubation,
500 slides were washed 3 times with PBS Tween 20 0.05% and incubated for 1 h
501 at room temperature with secondary antibodies diluted in PBS 1% donkey
502 serum. Following secondary antibodies were used: AF594-conjugated anti-goat

503 IgG, AF488-conjugated anti-rabbit IgG (both Jackson ImmunoResearch,
504 1:400). Finally, slides were washed, incubated with 0.5 µg/ml 4′,6 diamidine-2-
505 phenylindole (DAPI; Invitrogen) for 5 min, washed again and mounted with
506 ProlongDiamond medium (Invitrogen). The slides were scanned using the
507 automated multispectral microscopy system Vectra 3.0 (PerkinElmer). An
508 unstained slide was used to generate the spectral profile of autofluorescence
509 in studied tissues. The Inform software (PerkinElmer) was used for spectral
510 unmixing of individual fluorophores and autofluorescence.
511
512 *Flow cytometry*
513 Animals were euthanized by isoflurane overdose. The right heart ventricle was
514 perfused with 10 ml PBS to eliminate the blood from the lung vessels. Primary
515 tumors and lungs were collected in DMEM, cut into small pieces and digested
516 for 45 minutes at 37°C in DMEM containing 1 mg/ml collagenase IV and 2.6
517 *µ*g/ml DNase I (both Sigma) on a rotating device. Samples were washed with
518 PBS by centrifugation for 5 minutes at 350 *g*, the pellet was suspended in PBS
519 and filtered through a 70-µm filter (BD Biosciences) to obtain a single cell
520 suspension. For lymphocyte analysis, cells were further purified by
521 centrifugation over a Percoll gradient (GE Healthcare, 17-0891-01, Sigma
522 Aldrich).
523 Single cells were stained according to standard protocols. Briefly, cells were
524 surface-stained in 50 *µ*l antibody-mix in PBS. For intracellular cytokine staining,
525 cells were stimulated with 100 ng/ml phorbol 12-myristate 13-acetate (PMA)
526 plus 1 *µ*g/ml ionomycin for 4 h at 37°C in the presence of GolgiPlug/GolgiStop

527 (BD Pharmigen). Cells were stained for surface molecules as described above,
528 washed with PBS, and fixed for 30 min on ice using IC Fixation Buffer from
529 Foxp3/Transcription Factor Staining Buffer Set (eBioscience). Subsequently,
530 cells were stained for intracellular cytokines in permeabilization buffer from the
531 Foxp3/Transcription Factor Staining Buffer Set overnight at 4°C. After washing
532 with permeabilization buffer, samples were suspended in FACS buffer (PBS,
533 20 mM EDTA pH 8.0, 2% FCS) and acquired using a CyAn ADP9 flow
534 cytometer (Beckman Coulter), FACS LSRII Fortessa or FACSymphony (both
535 BD Biosciences). For quantitative analysis, CountBright absolute counting
536 beads were used (ThermoFisher Scientific). In all staining, dead cells were
537 excluded using Live/Dead fixable staining reagents (Invitrogen), and doublets
538 were excluded by FSC-A versus FSC-H and SSC-A versus SSC-H gating.
539 Following directly labelled anti-mouse primary antibodies were used: Anti-CD8a
540 in BUV 805, clone 53-6.7, rat IgG2a, BD. Anti-CD11b in BUV 661, clone M1/70,
541 rat IgG2b, BD. Anti-CD45.2 in BUV 653, clone 30-F11, rat IgG2b, BD. Anti-
542 VISTA in AF488, clone MH5A, armenian hamster IgG1, BioLegend. Anti-CD39
543 in PerCP-eFluor710, clone 24DMS1, rat IgG2b, ThermoFisher Scientific. Anti-
544 LAG3 in BV 421, clone C9B7W, rat IgG1, BioLegend. Anti-CD44 in BV 570,
545 clone IM7, rat IgG2b, BioLegend. Anti-CD73 in BV 605, clone TY/11.8, rat IgG1,
546 BioLegend. Anti-CD25 in BV 650, clone PC61, rat IgG1, BioLegend. Anti-PD-1
547 in BV 785, clone 29F.1A12, rat IgG2a, BioLegend. Anti-TCRβ in PE-Cy5, clone
548 H57-597, armenian hamster IgG1, BioLegend. Anti-KLRG1 in APC-Cy7, clone
549 2F1/KLRG1, armenian hamster IgG1, BioLegend. Anti-TIM3 in AF647, clone
550 B8.2C12, rat IgG1, BioLegend. Anti-CD103 in Biotin, clone 2E7, armenian

551 hamster IgG1, BioLegend. Anti-Streptavidin in BUV 395, BD. Anti-Ki67 in BV
552 480, clone B56, mouse IgG1, BD. Anti-TNFα in BV711, clone MP6-XT22, rat
553 IgG1, BioLegend. Anti-INFγ BUV 737, clone XMG1.2, rat IgG1, BD. Anti-CD4
554 in BUV 496, clone GK1.5, rat IgG2b, BD. Anti-FOXP3 in PE, clone FJK-16s, rat
555 IgG2a, ThermoFisher Scientific. Anti-EOMES in PE-eFluor610, clone
556 Dan11mag, rat IgG2a, ThermoFisher Scientific. Anti-T-bet in PE-Cy7, clone
557 eBio4B10, rat IgG1, ThermoFisher Scientific. Anti-CTLA4 in APC-AR700, clone
558 UC10-4F10-11, armenian hamster IgG1, BD. Anti-CD24 in FITC, clone M1/69,
559 rat IgG2b, BioLegend.
560 Flow cytometry data were compensated and exported using FlowJo software
561 (version 10, TreeStar Inc.). The exported FCS files were normalized using Cyt3
562 MATLAB (version 2017b) and uploaded into Rstudio (R software environment,
563 version 3.4.0). tSNE and FlowSOM algorithm mapping live cells from a pooled
564 sample were performed as described[74]. CellCNN was run using default
565 parameters, dividing data into training and validation steps as described[33].
566
567 *Purification of CD39$^+$PD-1$^+$CD8$^+$ T cells*
568 Primary tumors were processed as described under “Flow Cytometry”. After the
569 Percoll gradient, the leukocyte fraction was enriched for CD8$^+$ T cells using anti-
570 mouse CD8a microbeads (Miltenyi Biotec) and autoMACS equipment (Miltenyi
571 Biotec) according to the manufacturer’s instructions. Subsequently, cells were
572 stained for CD44, CD39, PD-1 and CD8 as described under “Flow Cytometry”
573 and live, single CD44$^+$CD39$^+$PD-1$^+$CD8$^+$ T cells as well as other CD44$^+$CD8$^+$ T
574 cells were sorted using an ARIA III Sorter (BD Biosciences).

575

576 *Adoptive transfer of CD39$^+$PD-1$^+$CD8$^+$ T cells*

577 Sorted cells were counted using trypan blue (Trypan Blue solution, Sigma
578 Aldrich) to exclude dead cells. Twohundred-thousand CD44$^+$CD39$^+$PD-1$^+$CD8$^+$
579 T cells were injected immediately after 10^5 4T07-LZ cells. Injections were given
580 intravenously.

581

582 *In vitro induction of senescence*

583 Twenty-thousand 4T07 cells were plated in a 6-well plate. Subsequently,
584 75 ng/ml mouse IFNγ (R&D Systems) plus 5 ng/ml mouse TNFα (PeproTech)
585 were added and cells were incubated at 37°C in a humidified atmosphere with
586 5% CO_2 for 6 days as described. The proportion of senescent cells was
587 determined by staining for β-galactosidase activity using Senescence β-
588 Galactosidase Staining Kit (9860, Cell Signaling Technology) as described[42].

589

590 *RNA-sequencing*

591 Library preparation: The libraries were prepared following the Smart-seq2
592 protocol[75]. Five-hundred pg of cDNA from each sample were tagmented and
593 amplified using Illumina Nextera XT kit. The resulting libraries were pooled,
594 double-sided size selected (0.5x followed by 0.8x ratio using Beckman Ampure
595 XP beads) and quantified using an Agilent 4200 TapeStation System. The pool
596 of libraries was sequenced in an Illumina NovaSeq6000 sequencer (single-end
597 100 bp) with a depth of around 20 Mio reads per sample as a service by the
598 Functional Genomics Center Zurich (FGCZ).

599 Data evaluation: The raw data generated by Illumina NovaSeq6000 sequencer
600 were analyzed using SUSHI, a framework for analysis of NGS data developed
601 by the FGCZ (Hatakeyama et al., 2016, Qi et al., 2017). Briefly, after quality
602 control, the reads were aligned to a reference genome (Ensembl genome
603 Mus_musculus. GRCm38 dated 2018.02.26) with STAR 2.7.3a. The software
604 package EdgeR was used to detect differentially expressed genes. We applied
605 a threshold of $p < 0.01$, FDR < 1% and a log fold-change of > 1.0 for
606 upregulated genes and < -1.0 for downregulated genes. Unsupervised
607 hierarchical clustering was done using the Ward2 method. Heatmaps were
608 generated with the software FunRich V3.1.3.
609 Gene set enrichment analysis[43,76] was performed on a list of genes ranked from
610 high to low estimated fold-change using the GSEA 4.0.3 Software (Broad
611 Institute) with enrichment statistic classic and 1000 permutations.
612
613 *Patient material*
614 Tumor tissues from 54 patients with breast cancer (Table 1) were collected at
615 the University Hospital Zurich, Switzerland. Donors provided written, informed
616 consent to tissue collection, analysis and data publication according to the
617 Declaration of Helsinki. Law abidance was reviewed and approved by the ethics
618 commission of the Canton Zurich (BASEC-Nr. 2018-02282 and KEK-ZH-2013-
619 0584). Samples were numerically coded to protect donors' rights to
620 confidentiality and privacy.
621
622 *Immunofluorescence of human samples*

623 Formalin-fixed paraffin-embedded samples were cut into 2 μm-thick sections
624 and dried overnight at 55°C. Antigen retrieval and deparaffinization were
625 performed in 1x Trilogy Solution (Cell Marque, 920P-06) for 15 minutes at
626 115°C. Staining was performed employing tyramide signal amplification (TSA)
627 and the Opal™ 7-color Manual IHC Kit (PerkinElmer). To prevent unspecific
628 binding of antibodies, slides were incubated with 4% donkey serum in PBS
629 (ANAWA BioWorld) in PBS/0.1% Triton X-100 for 15 minutes at 37°C. TSA
630 staining protocol was performed as described[77]. Briefly, slides were incubated
631 overnight at 4°C with primary antibody diluted in PBS/1% donkey serum/0.1%
632 Triton X-100. Subsequently, slides were washed in PBS Triton X-100 0.1% and
633 incubated with corresponding HRP-conjugated secondary antibodies.
634 Following primary antibodies were used: Anti-CD39 (mouse monoclonal
635 antibody, clone A1, BioLegend, 1:500), anti-PD-1 (rabbit monoclonal antibody,
636 clone D4W2J BioConcept, 1:4000), anti-CD8 (mouse monoclonal antibody,
637 clone RPA-T8, Cell Signaling, 1:2000), anti-PAN-Cytokeratin (rabbit polyclonal
638 antibody, cat. no. H-240, Santa Cruz, 1:2000) and anti-EpCAM (rabbit
639 monoclonal antibody, clone EPR20532-225, Abcam, 1:200). Following HRP-
640 conjugated secondary antibodies were used: anti-mouse IgG (H+L) (donkey
641 polyclonal antibody, 715-035-151 Jackson ImmunoResearch 1:500) and anti-
642 rabbit IgG (H+L) (donkey polyclonal antibody, 715-035-152 Jackson
643 ImmunoResearch 1:1000). Fluorescent signal was developed using the Opal™
644 7-color Manual IHC Kit. Finally, slides were washed, incubated with 0.5 μg/ml
645 4′,6-diamidine-2-phenylindole (DAPI; Invitrogen) for 5 min, washed again and
646 mounted with ProlongDiamond medium (Invitrogen). The slides were scanned

647 using the automated multispectral microscopy system Vectra 3.0
648 (PerkinElmer). An unstained slide was used to generate the spectral profile of
649 autofluorescence in studied tissues. The Inform software (PerkinElmer) was
650 used for (i) unmixing the spectra of individual fluorophores and
651 autofluorescence, (ii) performing automated tissue and cell segmentation into
652 tumor and non-tumor cells, and (iii) exporting single-cell intensity values for all
653 fluorescent signals. Single-cell parameter files were transformed into .fcs files
654 using R script (version 3.6.1) involving FlowCore and Biobase packages and
655 were analyzed using FlowJo software to gate on $CD39^+PD\text{-}1^+CD8^+$ T cell
656 populations in tumor tissue category (Supplemental Figure 7F). Gates were set
657 based on the intensity values identified in the fluorescent images. Cell density
658 values were measured as number of cells/mm^2 obtained as cell counts from the
659 gated populations divided by the tumor tissue area measured in the
660 corresponding patient. Samples were analyzed blinded.
661
662 *Statistical analysis*
663 Data were analyzed using GraphPad Prism 8.0 for Windows or Mac, and
664 RStudio (version 1.2.5019). For comparison of 2 experimental groups, 2-tailed
665 Student's t test with Welch's correction was performed. More than 2 groups
666 were compared using an ANOVA test with Bonferroni's correction. Data
667 following a logarithmic distribution (i.e. IVIS signal) were log transformed prior
668 to analysis. The number of mice per experimental group was determined based
669 on our previous experience with similar models. Every point represents one
670 mouse. Unless stated otherwise, data are shown as mean ± SD. $p < 0.05$ is

671 considered significant throughout. *$p < 0.05$, **$p < 0.01$, ***$p < 0.001$, ****$p <$
672 0.0001. CellCnn data were analyzed using the Kolmogorov–Smirnov two-
673 sample statistical test. In addition, the population identified by the algorithm was
674 compared in the two groups using the 2-tailed Student's t test with Welch's
675 correction.
676 Density of $CD39^+PD\text{-}1^+CD8^+$ T cells was correlated with the clinicopathological
677 information of the patients using corresponding R packages. Disease-free
678 survival was analyzed by Kaplan-Meier curve and log-rank test (Survminer and
679 Survival R packages), as well as univariate and multivariate Cox regression
680 (pROC, ROCR and Survival R packages). The threshold of $CD39^+PD\text{-}$
681 1^+CD8^+ or $CD8^+$ T cell density was identified by the Receiver Operating
682 Characteristics (ROC) curve analysis using 3-year disease-free survival for
683 defining long- and short-term survivors. Following values apply: Intra-tumoral
684 $CD39^+PD\text{-}1^+CD8^+$ T cells, 4.20; extra-tumoral $CD39^+PD\text{-}1^+CD8^+$ T cells, 8.43;
685 total $CD39^+PD\text{-}1^+CD8^+$ T cells, 5.71; intra-tumoral $CD8^+$ T cells, 249.20; extra-
686 tumoral $CD8^+$ T cells, 1218.60; total $CD8^+$ T cells, 562.29.
687
688 **Data deposition**
689
690 https://www.ncbi.nlm.nih.gov/sra/PRJNA609233
691
692 **Materials Availability**
693

All unique reagents generated in this study are available from the Lead Contact upon request.

696 **Legends to the figures**

697

698 **Figure 1. 4T07 but not 4T1 breast cancer cells are dormant after**
699 **dissemination to the lungs.**

700 **(A)** Diagram of the origin of 4T1 and 4T07 cell lines[21]. **(B)** Experimental design.
701 4T07-mCh cells (10^5) or PBS were injected into the mammary fat pad of female
702 BALB/c mice. Analysis was performed 30 d later. **(C)** Quantification of
703 disseminated 4T07-mCh cells by quantitative pathology. **(D)** 4T07-mCh cells
704 (10^5) were injected into the mammary fat pad of female BALB/c mice. Analysis
705 was performed 35 d later. Representative section of the primary tumor (upper
706 panels) and lung (lower panels) at the endpoint. Disseminated 4T07 cells were
707 detected as single, Ki67-negative cells in the lungs of 5 out of 5 mice.
708 Disseminated 4T07 cells are shown in red, Ki67 in green, DAPI in blue. Scale
709 bar indicates 50 μm. **(E)** Experimental design. 4T1 or 4T07 cells (10^5) were
710 injected into the mammary fat pad of female BALB/c mice. The tumor was
711 resected 20 d after injection and analysis was performed 21 d after resection
712 (endpoint). **(F)** Representative section of the lung at the endpoint. Disseminated
713 4T07 cells were detected as single, Ki67-negative cells in the lungs of 5 out of
714 5 mice. Disseminated 4T07 cells are shown in red, Ki67 in green, DAPI in blue.
715 Scale bar indicates 20 μm.

716 Each symbol represents an individual mouse. Five mice per group. *$p < 0.05$,
717 ***$p < 0.001$ (2-tailed Student's t-test). The bar represents the mean ± SD.
718 Results are representative of 3 independent experiments.

719

720 **Figure 2. Induction of protective immunity by the primary tumor mediates**
721 **metastatic dormancy.**
722 **(A)** Experimental design. 4T1 or 4T07 cells ($3x10^5$) were injected i.v. into female
723 BALB/c mice. Analysis was performed 25 d later. **(B)** Metastatic load in the
724 lungs determined by counting nodules. **(C)** Experimental design. 4T1 or 4T07
725 cells (10^5) were injected into the mammary fat pad of female BALB/c (*n*=5) or
726 BALB/c *Foxn1*$^{nu/nu}$ (*n*=7) mice. Analysis was performed 30 d later. Lungs of "WT
727 Late" mice (*n*=4) were analyzed when the 4T07 tumor size reached the size of
728 the BALB/c *Foxn1*$^{nu/nu}$ group, e.g. 35 days after tumor cell injection. **(D)** Weight
729 of primary tumors. Left panel with closed symbols, 4T1; right panel with open
730 symbols, 4T07. **(E)** Metastatic load in the lungs determined by counting
731 nodules. Left panel with closed symbols, 4T1; right panel with open symbols,
732 4T07. **(F)** Experimental design. Female BALB/c mice received 0.5 mg anti-CD8
733 or isotype control i.p. at days -1 and +5 relative to injection of 10^5 4T07-mCh
734 cells in the mammary fat pad. Analysis was performed 25 d later. **(G)** Metastatic
735 load in the lungs measured by bioluminescence. **(H)** Bioluminescence images.
736 **(I)** Experimental design. 4T07 cells (10^5) or PBS were injected into the
737 mammary fat pad of female BALB/c mice on d 0. On d 11, $3x10^5$ 4T07-LZ cells
738 were injected i.v. and analysis of lung metastatic load was performed on d 25.
739 We chose d 11 because, on the one hand, this gives T cells enough time to be
740 primed and expanded; on the other hand, it allows a long enough follow up after
741 i.v. injection without the risk that the size of the primary tumor reached the
742 humane endpoint of 225 mm^2, which would result in forced termination of the
743 experiment. **(J)** Quantification of lung metastatic load by bioluminescence. **(K)**

744 Bioluminescence images. **(L)** 4T07 cells (10^5) or PBS were injected into the
745 mammary fat pad of female BALB/c mice on d 0. On day 8, mice were injected
746 i.p. with 500 μg anti-CD8 or isotype control. On d 15, $3x10^5$ 4T07-LZ cells were
747 i.v. injected and lung metastatic load was quantified on d 25. **(M)** Quantification
748 of the lung metastatic load by bioluminescence on d 25.
749 Each symbol represents an individual mouse. $^{**}p < 0.01$, $^{****}p < 0.0001$, ns =
750 not significant (2-tailed Student's t-test with Welch's correction (B, D left panel,
751 E left panel, G, J), ANOVA with Bonferroni correction (D right panel, E right
752 panel, M). The bar represents the mean ± SD. Results are representative of at
753 least 2 independent experiments.
754
755 **Figure 3. CD39$^+$PD-1$^+$CD8$^+$ T cells emerge in dormant breast cancer.**
756 Female BALB/c mice were injected with 10^5 4T1 or 4T07 cells in the mammary
757 fat pad and primary tumors were analyzed by flow cytometry 20 d later (*n*=4).
758 **(A)** t-SNE visualization of markers after gating on single, live, CD45$^+$ TCRβ$^+$
759 CD44$^+$ cells. **(B)** Upper panel: t-SNE plots of the main T cell subsets. Lower left
760 panel: Frequency of the main T cell subsets in both groups. Each symbol
761 represents an individual mouse. Lower right panel: Heat map with marker
762 expression of the main T cell subsets. **(C)** t-SNE visualization of markers on
763 CD8$^+$ TCRβ$^+$ cells. **(D)** Upper panel: t-SNE plots of the main CD8$^+$ T cell subsets
764 identified by FlowSOM algorithm. Lower panel: Frequency of the main CD8$^+$ T
765 subsets identified by FlowSOM algorithm in both groups. **(E)** Scaled histograms
766 of arcsinh-transformed marker expression showing the relative marker
767 distribution of the population identified by CellCnn (red) among all CD8$^+$ T cells

768 (blue). KS indicates the Kolmogorov–Smirnov two-sample test between the
769 whole-cell population and the selected cell subsets. **(F)** Heat map with marker
770 expression of the main CD8$^+$ T cell subsets identified by FlowSOM algorithm.
771 **(G)** Representative FACS plot of 4T1 and 4T07 primary tumors after gating on
772 CD8$^+$ TCRβ$^+$. **(H)** Frequency of the population of total CD8$^+$ identified by
773 CellCnn in both models. **(I)** The number of CD39$^+$PD-1$^+$CD8$^+$ T cells in the
774 lungs. **(J)** Representative CD103-staining of live CD39$^+$PD-1$^+$CD8$^+$ T cells from
775 the lungs.
776 Each symbol represents an individual mouse. *$p < 0.05$, ****$p < 0.0001$ (2-tailed
777 Student's t-test with Welch's correction). The bar represents the mean ± SD.
778
779 **Figure 4. Tumor-associated CD39$^+$PD-1$^+$CD8$^+$ T cells prevent metastatic**
780 **outgrowth**.
781 **(A)** Experimental design. 4T07-mCh cells (10^5) were injected into the mammary
782 fat pad of female BALB/c mice. The breast tumor was resected on d 20 and
783 histological analysis of lungs was performed on d 32. Mice received an i.p.
784 injection with 250 μg anti-PD-1 or isotype control on d 15, 18, 23, 26 and 29.
785 **(B)** Enumeration of disseminated 4T07 cells by quantitative pathology (right
786 panel). Each symbol represents an individual mouse. *$p < 0.05$, (2-tailed
787 Student's t-test with Welch's correction). The bar represents the mean ± SD.
788 **(C)** Gating used for sorting of CD44$^+$CD39$^+$PD-1$^+$CD8$^+$ and the rest of the
789 CD44$^+$CD8$^+$ population (termed other CD8$^+$ T cells) from established 4T07
790 orthotopic breast tumors. **(D)** Experimental design. Two-hundred-thousand
791 sorted CD44$^+$CD39$^+$PD-1$^+$CD8$^+$ or other CD44$^+$CD8$^+$ T cells were transferred

792 after injection of 10^5 4T07-LZ cells into female BALB/c mice. All injections were
793 given intravenously. Lung metastatic load was determined by bioluminescence
794 14 d later. **(E)** Bioluminescence of lungs at endpoint. **(F)** Quantification of lung
795 metastatic load by bioluminescence. **(G)** Experimental design. 4T07-mCh cells
796 (10^5) were injected into the mammary fat pad of female BALB/c mice. Mice
797 received an i.p. injection with 500 μg anti-IFNγ plus 500 μg anti-TNFα every 3rd
798 day. Control mice received isotype control antibody. On d 20, 4T07 cells were
799 visualized in lungs by immunofluorescence. **(H)** Two representative examples
800 showing clusters of proliferating 4T07 cells in the lungs of mice treated with
801 anti-IFNγ plus anti-TNFα. Proliferating 4T07 cells were detected in the lungs
802 from 4 out of 8 mice.
803 Each symbol represents an individual mouse. Five mice per group. $^{**}p < 0.01$,
804 $^{***}p < 0.001$ (ANOVA with Bonferroni's correction). The bar represents the
805 mean ± SD.
806
807 **Figure 5. CD39$^+$PD-1$^+$CD8$^+$ T cells have a unique transcriptional signature.**
808 **(A)** Hierarchical clustering of significantly differentially expressed genes
809 comparing CD44$^+$CD39$^+$PD-1$^+$CD8$^+$ and rest of CD44$^+$CD8$^+$ T cells sorted from
810 4T1 and 4T07 breast tumors. **(B)** Volcano plot comparing transcripts in
811 CD44$^+$CD39$^+$PD-1$^+$CD8$^+$ T cells with those in other CD44$^+$CD8$^+$ T cells sorted
812 from 4T07 breast tumors. The red symbols represent transcripts that are
813 significantly over-expressed in CD44$^+$CD39$^+$PD-1$^+$CD8$^+$ T cells, whereas the
814 blue symbols represent significantly under-expressed transcripts. **(C)** Heat map
815 showing relative expression of selected transcripts in CD44$^+$CD39$^+$PD-1$^+$CD8$^+$

816 (three top rows) and other CD44$^+$CD8$^+$ T cells (three bottom rows) identified by
817 differential gene expression analysis. **(D)** Gene set enrichment analysis
818 comparing the transcriptional profile to the data published by Goldrath et al.[78]
819 et al (left panel) and Savas et al.[19] (right panel).
820
821 **Figure 6. High density of intra-tumoral CD39$^+$PD-1$^+$CD8$^+$ but not total CD8$^+$**
822 **T cells correlates with disease-free survival in human breast cancer.**
823 **(A)** Representative images of 5-color multiplex immunofluorescence on human
824 breast cancer. Staining shows epithelial cells (PanCK + EpCAM, yellow), CD8$^+$
825 T cells (CD8, magenta), PD-1 (green), CD39 (red) and nuclear staining (DAPI,
826 blue). Scale bar is 50 μm. **(B)** Disease-free survival of 54 patients with high or
827 low number of intra-tumoral CD39$^+$PD-1$^+$CD8$^+$ T cells**. (C)** Disease-free survival
828 of 54 patients with high or low number of intra-tumoral CD8$^+$ T cells. The
829 threshold for separating patients with high and low CD39$^+$PD-1$^+$CD8$^+$ T cell
830 densities was defined using ROC curve analysis.

831 **Legends to the supplemental figures**

832

833 **Supplemental Figure S1. Circulating and disseminated cancer cells in**
834 **mice with 4T1 or 4T07 orthotopic tumors**.

835 **(A)** Experimental design. 4T1 or 4T07 cells (10^5) were injected into the
836 mammary fat pad of female BALB/c mice. Analysis was performed 30 d later.
837 **(B)** Growth curve of primary breast cancer. **(C)** Representative images of lungs
838 at the endpoint stained with India ink to macroscopically visualize metastatic
839 nodules. **(D)** The number of metastatic nodules in the lungs. **(E)** BALB/c mice
840 were injected with 10^5 4T1 or 4T07 cells in the mammary fat pad and
841 disseminated cancer cells (DCCs) were detected by colony-forming assay in
842 the lungs 30 d later. DCCs were detected in all mice (n=5 per group).
843 Representative images of colonies from cultured lung-digests are shown. **(F)**
844 4T07-mCh cells (10^5) were injected into the mammary fat pad of female BALB/c
845 mice. Analysis was performed 35 d later. Disseminated 4T07 cells were found
846 in 5/5 mice and are shown in red, Ki67 in green, DAPI in blue. Representative
847 pictures from a cohort of 5 mice. Scale bar: 20 μm.
848 Results are representative of 3 independent experiments.

849

850 **Supplemental Figure S2. 4T07 and 4T1 induce similar systemic**
851 **inflammation**.

852 Female BALB/c mice were injected with 10^5 4T1 or 4T07 cells in the mammary
853 fat pad. Control mice were injected with PBS. Analysis was performed at the
854 indicated days after cancer cell injection. **(A)** Spleen weight. **(B)** Percentage

855 circulating neutrophils of $CD45^+$ cells. **(C-F)** Total number of cells per mg lung
856 tissue: inflammatory monocytes (C), neutrophils (D), eosinophils (E), alveolar
857 macrophages (F). **(G)** Female BALB/c mice were injected with 10^5 4T1 cells
858 into the mammary fat pad. The plots show a representative gating strategy of
859 lungs processed 20 d after tumor cell injection.
860 Each symbol represents an individual mouse. Five mice per group. ns = not
861 significant (2-tailed Student's t-test with Welch's correction). The bar represents
862 the mean ± SD.
863
864 **Supplemental Figure S3. 4T07 breast cancer elicits systemic protective**
865 **immunity.**
866 **(A)** 4T07 cells (10^5) or PBS were injected into the mammary fat pad of female
867 BALB/c mice on d 0. On d 11, $3x10^5$ 4T07-LZ cells were injected i.v., and lung
868 metastatic load (seeding) was quantified by bioluminescence 30 min and 3 h
869 later. **(B)** Bioluminescence images. ns = not significant (2-tailed Student's t-test
870 with Welch's correction). Each symbol represents an individual mouse. The bar
871 represents the mean ± SD. Results are representative of 2 independent
872 experiments. **(C)** Experimental design. 4T07 cells (10^5) or PBS were injected
873 into the mammary fat pad of female BALB/c mice on d 0. On d 11, 10^5 4T07-
874 mCh cells were injected i.v. and analysis of lung metastatic load was performed
875 on d 25. **(D)** Representative section of the lung at the endpoint. Upper panels:
876 Disseminated 4T07 cells were detected as single, Ki67-negative cells in the
877 lungs of 5 out of 5 mice. Disseminated 4T07 cells are shown in red, DAPI in
878 blue. Lower panels: 4T07-metastatic nodules. Macro-metastasis was detected

879 in 5 out of 5 mice. Scale bar indicates 20 μm. **(E)** Experimental design. 4T07
880 cells (10^5) or PBS were injected into the mammary fat pad of female BALB/c
881 mice on d 0. The tumor was resected on d 8; PBS-injected mice and one group
882 of 4T07-injected mice underwent mock resection. On d 15, 10^5 4T07-mCh cells
883 were injected i.v., and analysis of lung metastatic load was performed on d 30.
884 **(F)** Macroscopic pictures of lungs. Upper row: Metastatic nodules seen in
885 magnifications of the circled areas. Middle and lower row: Absence of
886 macroscopically visible metastatic nodules. **(G)** Representative example of
887 disseminated 4T07 cells present in the lungs as single, Ki67-negative cells.
888 Disseminated 4T07 cells are shown in red, Ki67 in green, DAPI in blue. Scale
889 bar indicates 20 μm (upper panels) or 100 μm (lower panels). **(H)** Experimental
890 design. 4T07 cells (10^5) or PBS were injected into the mammary fat pad of
891 female BALB/c mice on d 0. The tumor was resected on d 8 (PBS-injected mice
892 underwent mock surgery) and $3x10^5$ 4T07-LZ cells were i.v. injected on d 15.
893 The lung metastatic load was quantified on d 30. **(I)** Quantification of lung
894 metastatic load by bioluminescence. ****$p < 0.0001$, (2-tailed Student's t-test
895 with Welch's correction). Each symbol represents an individual mouse. The bar
896 represents the mean ± SD. Results are representative of 2 independent
897 experiments. **(J)** Experimental design. 4T1 cells (10^5), 4T07 cells (10^5) or PBS
898 were injected into the mammary fat pad of female BALB/c mice on d 0. On d
899 11, $3x10^5$ 4T1-LZ cells were injected and analysis of lung metastatic load was
900 performed on d 25. **(K)** Quantification of lung metastatic load by
901 bioluminescence. *$p < 0.05$, ****$p < 0.0001$, ns = not significant (ANOVA with

902 Bonferroni correction). Each symbol represents an individual mouse. The bar
903 represents the mean ± SD.
904
905 **Supplemental Figure S4. Expression of selected markers by CD39$^+$PD-**
906 **1$^+$CD8$^+$ T cells.**
907 Female BALB/c mice were injected with 10^5 4T1 or 4T07 cells in the mammary
908 fat pad and primary tumors were analyzed by flow cytometry 20 d later (*n*=4).
909 **(A)** Gating strategy for Figure 3. **(B)** Representative examples of expression of
910 selected markers on live, single CD45$^+$ CD44$^+$TCRβ$^+$CD11b$^-$CD39$^+$PD-1$^+$CD8$^+$
911 T cells. **(C)** Representative examples of IFNγ and TNFα production by
912 CD45$^+$CD44$^+$TCRβ$^+$CD11b$^-$CD39$^+$PD-1$^+$CD8$^+$ T cells sorted from 4T07 tumors
913 after in vitro stimulation with 100 ng/ml phorbol 12-myristate 13-acetate (PMA)
914 plus 1 *μ*g/ml ionomycin for 4 h at 37°C in the presence of GolgiPlug/GolgiStop.
915
916 **Supplemental Figure S5. IFNγ and TNFα induce senescence of 4T07 cells.**
917 Twenty-thousand 4T07 cells were plated in a 6-well plate. Subsequently,
918 75 ng/ml mouse IFNγ plus 5 ng/ml mouse TNFα were added and cells were
919 incubated for 6 days. **(A)** Proportion of senescent cells in control and IFNγ plus
920 TNFα-exposed 4T07 cells. Each symbol represents an individual culture. $^{**}p <$
921 0.01 (2-tailed Student's t-test with Welch's correction). The bar represents the
922 mean ± SD. Results are representative of 2 independent experiments. **(B)**
923 Representative examples of staining for SA-β-galactosidase activity (blue) as
924 proxy for senescence. Left panel, medium. Right panel, IFNγ plus TNFα.
925

926 **Supplemental Figure S6. CD39$^+$PD-1$^+$CD8$^+$ T cells in dormant and**
927 **metastatic tumors have a similar transcription signature.**
928 **(A)** Hierarchical clustering of all genes by sorted CD44$^+$CD39$^+$PD-1$^+$CD8$^+$ and
929 CD44$^+$CD8$^+$ T cells. **(B)** Volcano plot comparing transcripts in CD44$^+$CD39$^+$PD-
930 1$^+$CD8$^+$ T cells sorted from 4T07 breast tumors with those sorted from 4T1
931 breast tumors. The red symbols represent transcripts that are significantly
932 overexpressed in CD44$^+$CD39$^+$PD-1$^+$CD8$^+$ T cells from 4T07 breast tumors,
933 whereas the blue symbols represent significantly under-expressed transcripts.
934 **(C, D)** Venn diagram showing **(C)** shared or **(D)** significantly differentially
935 expressed genes in CD44$^+$CD39$^+$PD-1$^+$CD8$^+$ and CD44$^+$CD8$^+$ T cells sorted
936 from 4T1 and 4T07 breast cancers.
937
938 **Supplemental Figure S7. High density of intra-tumoral CD39$^+$PD-1$^+$CD8$^+$**
939 **but not total CD8$^+$ T cells correlate with disease-free survival in human**
940 **luminal A and B breast cancer.**
941 **(A)** Disease-free survival of patients with luminal A, luminal B or triple-negative
942 (TN) breast cancer. **(B)** Disease-free survival of 54 patients with high or low
943 number of extra-tumoral CD39$^+$PD-1$^+$CD8$^+$ T cells. **(C)** Disease-free survival of
944 54 patients with high or low number of intra-tumoral + extra-tumoral CD39$^+$PD-
945 1$^+$CD8$^+$ T cells. **(D)** Disease-free survival of 20 luminal A and 25 luminal B
946 breast cancer patients with high or low number of intra-tumoral CD39$^+$PD-
947 1$^+$CD8$^+$ T cells**. (E)** Disease-free survival of 20 luminal A and 25 luminal B
948 breast cancer patients with high or low number of intra-tumoral CD8$^+$ T cells**.**
949 ns = not significant. **(F)** Representative example of a sample with high (upper

950 panels) or low (lower panels) number of intra-tumoral $CD39^+PD\text{-}1^+CD8^+$ T cells.
951 Single-cell parameter files were transformed into .fcs files using R studio and
952 were analyzed using FlowJo software. Values of number of cells/mm^2 were
953 obtained by using the values of total counts obtained from the FlowJo analysis
954 and the measurements of tumor tissue area obtained from the inform analysis.
955 The threshold for separating patients with high and low $CD39^+PD\text{-}1^+CD8^+$ T cell
956 densities was defined using ROC curve analysis.

957 1. Kennecke, H. *et al.* Metastatic behavior of breast cancer subtypes. *J.*
958 *Clin. Oncol.* (2010) doi:10.1200/JCO.2009.25.9820.
959 2. Colzani, E. *et al.* Time-dependent risk of developing distant metastasis
960 in breast cancer patients according to treatment, age and tumour
961 characteristics. *Br. J. Cancer* (2014) doi:10.1038/bjc.2014.5.
962 3. Pan, H. *et al.* 20-year risks of breast-cancer recurrence after stopping
963 endocrine therapy at 5 years. *N. Engl. J. Med.* (2017)
964 doi:10.1056/NEJMoa1701830.
965 4. Karrison, T. G., Ferguson, D. J. & Meier, P. Dormancy of mammary
966 carcinoma after mastectomy. *J. Natl. Cancer Inst.* (1999)
967 doi:10.1093/jnci/91.1.80.
968 5. Demicheli, R., Abbattista, A., Miceli, R., Valagussa, P. & Bonadonna, G.
969 Time distribution of the recurrence risk for breast cancer patients
970 undergoing mastectomy: Further support about the concept of tumor
971 dormancy. *Breast Cancer Res. Treat.* (1996) doi:10.1007/BF01807163.
972 6. Sosa, M. S., Bragado, P. & Aguirre-Ghiso, J. A. Mechanisms of
973 disseminated cancer cell dormancy: an awakening field. *Nat Rev*
974 *Cancer* **14**, 611–622 (2014).
975 7. Braun, S. *et al.* A pooled analysis of bone marrow micrometastasis in
976 breast cancer. *N. Engl. J. Med.* (2005) doi:10.1056/NEJMoa050434.
977 8. Janni, W. *et al.* Persistence of disseminated tumor cells in the bone
978 marrow of breast cancer patients predicts increased risk for relapse - A
979 European pooled analysis. *Clin. Cancer Res.* (2011) doi:10.1158/1078-
980 0432.CCR-10-2515.

981 9. Balz, L. M. *et al.* The interplay of HER2/HER3/PI3K and
982 EGFR/HER2/PLC-γ1 signalling in breast cancer cell migration and
983 dissemination. *J. Pathol.* (2012) doi:10.1002/path.3991.
984 10. Ranganathan, A. C., Zhang, L., Adam, A. P. & Aguirre-Ghiso, J. A.
985 Functional coupling of p38-induced up-regulation of BiP and activation
986 of RNA-dependent protein kinase-like endoplasmic reticulum kinase to
987 drug resistance of dormant carcinoma cells. *Cancer Res.* (2006)
988 doi:10.1158/0008-5472.CAN-05-3092.
989 11. Ghajar, C. M. Metastasis prevention by targeting the dormant niche.
990 *Nature Reviews Cancer* (2015) doi:10.1038/nrc3910.
991 12. Ghajar, C. M. *et al.* The perivascular niche regulates breast tumour
992 dormancy. *Nat Cell Biol* **15**, 807–817 (2013).
993 13. Bragado, P. *et al.* TGF-β2 dictates disseminated tumour cell fate in
994 target organs through TGF-β-RIII and p38α/β signalling. *Nat. Cell Biol.*
995 (2013) doi:10.1038/ncb2861.
996 14. Hagerling, C. *et al.* Immune effector monocyte–neutrophil cooperation
997 induced by the primary tumor prevents metastatic progression of breast
998 cancer. *Proc. Natl. Acad. Sci. U. S. A.* (2019)
999 doi:10.1073/pnas.1907660116.
1000 15. Malladi, S. *et al.* Metastatic Latency and Immune Evasion through
1001 Autocrine Inhibition of WNT. *Cell* **165**, 45–60 (2016).
1002 16. Eyles, J. *et al.* Tumor cells disseminate early, but immunosurveillance
1003 limits metastatic outgrowth, in a mouse model of melanoma. *J Clin*
1004 *Invest* **120**, 2030–2039 (2010).

1005 17. Pommier, A. *et al.* Unresolved endoplasmic reticulum stress engenders
1006 immune-resistant, latent pancreatic cancer metastases. *Science (80-.).*
1007 (2018) doi:10.1126/science.aao4908.
1008 18. Ali, H. R. *et al.* Association between CD8+ T-cell infiltration and breast
1009 cancer survival in 12 439 patients. *Ann. Oncol.* (2014)
1010 doi:10.1093/annonc/mdu191.
1011 19. Savas, P. *et al.* Single-cell profiling of breast cancer T cells reveals a
1012 tissue-resident memory subset associated with improved prognosis.
1013 *Nat. Med.* (2018) doi:10.1038/s41591-018-0078-7.
1014 20. Simoni, Y. *et al.* Bystander CD8 + T cells are abundant and
1015 phenotypically distinct in human tumour infiltrates. *Nature* (2018)
1016 doi:10.1038/s41586-018-0130-2.
1017 21. Aslakson, C. J. & Miller, F. R. Selective events in the metastatic process
1018 defined by analysis of the sequential dissemination of subpopulations of
1019 a mouse mammary tumor. *Cancer Res* **52**, 1399–1405 (1992).
1020 22. Pulaski, B. A. & Ostrand-Rosenberg, S. Mouse 4T1 Breast Tumor
1021 Model. in *Current Protocols in Immunology* (2001).
1022 doi:10.1002/0471142735.im2002s39.
1023 23. Beffinger, M. *et al.* CSF1R-dependent myeloid cells are required for
1024 NKmediated control of metastasis. *JCI Insight* **3**, (2018).
1025 24. Carlson, P. *et al.* Targeting the perivascular niche sensitizes
1026 disseminated tumour cells to chemotherapy. *Nat. Cell Biol.* (2019)
1027 doi:10.1038/s41556-018-0267-0.
1028 25. Peinado, H. *et al.* Pre-metastatic niches: organ-specific homes for

1029 metastases. *Nat Rev Cancer* **17**, 302–317 (2017).
1030 26. Spiegel, A. *et al.* Neutrophils Suppress Intraluminal NK Cell-Mediated
1031 Tumor Cell Clearance and Enhance Extravasation of Disseminated
1032 Carcinoma Cells. *Cancer Discov* **6**, 630–649 (2016).
1033 27. Kowanetz, M. *et al.* Granulocyte-colony stimulating factor promotes lung
1034 metastasis through mobilization of Ly6G+Ly6C+ granulocytes. *Proc Natl*
1035 *Acad Sci U S A* **107**, 21248–21255 (2010).
1036 28. Ouzounova, M. *et al.* Monocytic and granulocytic myeloid derived
1037 suppressor cells differentially regulate spatiotemporal tumour plasticity
1038 during metastatic cascade. *Nat. Commun.* (2017)
1039 doi:10.1038/ncomms14979.
1040 29. Sharma, S. K. *et al.* Pulmonary Alveolar Macrophages Contribute to the
1041 Premetastatic Niche by Suppressing Antitumor T Cell Responses in the
1042 Lungs. *J. Immunol.* (2015) doi:10.4049/jimmunol.1403215.
1043 30. Van Der Maaten, L. & Hinton, G. Visualizing data using t-SNE. *J. Mach.*
1044 *Learn. Res.* (2008).
1045 31. Van Gassen, S. *et al.* FlowSOM: Using self-organizing maps for
1046 visualization and interpretation of cytometry data. *Cytom. Part A* (2015)
1047 doi:10.1002/cyto.a.22625.
1048 32. Weber, L. M. & Robinson, M. D. Comparison of clustering methods for
1049 high-dimensional single-cell flow and mass cytometry data. *Cytom. Part*
1050 *A* (2016) doi:10.1002/cyto.a.23030.
1051 33. Arvaniti, E. & Claassen, M. Sensitive detection of rare disease-
1052 Associated cell subsets via representation learning. *Nat. Commun.*

1053 (2017) doi:10.1038/ncomms14825.

1054 34. Krieg, C. *et al.* High-dimensional single-cell analysis predicts response
1055 to anti-PD-1 immunotherapy. *Nat Med* **24**, 144–153 (2018).

1056 35. Anderson, A. C., Joller, N. & Kuchroo, V. K. Lag-3, Tim-3, and TIGIT:
1057 Co-inhibitory Receptors with Specialized Functions in Immune
1058 Regulation. *Immunity* **44**, 989–1004 (2016).

1059 36. Pandiyan, P., Hegel, J. K. E., Krueger, M., Quandt, D. & Brunner-
1060 Weinzierl, M. C. High IFN-γ Production of Individual CD8 T
1061 Lymphocytes Is Controlled by CD152 (CTLA-4). *J. Immunol.* **178**, 2132–
1062 2140 (2007).

1063 37. Workman, C. J. *et al.* Lymphocyte Activation Gene-3 (CD223)
1064 Regulates the Size of the Expanding T Cell Population Following
1065 Antigen Activation In Vivo. *J. Immunol.* **172**, 5450–5455 (2004).

1066 38. Koyama, S. *et al.* Adaptive resistance to therapeutic PD-1 blockade is
1067 associated with upregulation of alternative immune checkpoints. *Nat.*
1068 *Commun.* **7**, 1–9 (2016).

1069 39. Clarke, J. *et al.* Single-cell transcriptomic analysis of tissue-resident
1070 memory T cells in human lung cancer. *J. Exp. Med.* (2019)
1071 doi:10.1084/jem.20190249.

1072 40. Park, C. O. & Kupper, T. S. The emerging role of resident memory T
1073 cells in protective immunity and inflammatory disease. *Nature Medicine*
1074 (2015) doi:10.1038/nm.3883.

1075 41. Egelston, C. A. *et al.* Resident memory CD8+ T cells within cancer
1076 islands mediate survival in breast cancer patients. *JCI Insight* (2019)

1077 doi:10.1172/jci.insight.130000.
1078 42. Braumuller, H. *et al.* T-helper-1-cell cytokines drive cancer into
1079 senescence. *Nature* **494**, 361–365 (2013).
1080 43. Subramanian, A. *et al.* Gene set enrichment analysis: A knowledge-
1081 based approach for interpreting genome-wide expression profiles. *Proc.*
1082 *Natl. Acad. Sci. U. S. A.* (2005) doi:10.1073/pnas.0506580102.
1083 44. Scott, A. C. *et al.* TOX is a critical regulator of tumour-specific T cell
1084 differentiation. *Nature* (2019) doi:10.1038/s41586-019-1324-y.
1085 45. Costa-Silva, B. *et al.* Pancreatic cancer exosomes initiate pre-
1086 metastatic niche formation in the liver. *Nat Cell Biol* **17**, 816–826 (2015).
1087 46. Wculek, S. K. & Malanchi, I. Neutrophils support lung colonization of
1088 metastasis-initiating breast cancer cells. *Nature* **528**, 413–417 (2015).
1089 47. Duhen, T. *et al.* Co-expression of CD39 and CD103 identifies tumor-
1090 reactive CD8 T cells in human solid tumors. *Nat. Commun.* (2018)
1091 doi:10.1038/s41467-018-05072-0.
1092 48. Wagner, J. *et al.* A Single-Cell Atlas of the Tumor and Immune
1093 Ecosystem of Human Breast Cancer. *Cell* (2019)
1094 doi:10.1016/j.cell.2019.03.005.
1095 49. Yan, J. *et al.* Control of metastases via myeloid CD39 and NK cell
1096 effector function. *Cancer Immunol. Res.* (2020) doi:10.1158/2326-
1097 6066.CIR-19-0749.
1098 50. Li, X. Y. *et al.* Targeting CD39 in cancer reveals an extracellular ATP-
1099 and inflammasome-driven tumor immunity. *Cancer Discov.* (2019)
1100 doi:10.1158/2159-8290.CD-19-0541.

1101 51. Canale, F. P. *et al.* CD39 expression defines cell exhaustion in tumor-
1102 infiltrating CD8+ T cells. *Cancer Res.* (2018) doi:10.1158/0008-
1103 5472.CAN-16-2684.
1104 52. Egelston, C. *et al.* Complex phenotyping of PD-1+ CD39+ exhausted
1105 CD8+ T cells in human carcinomas. *J. Immunol.* (2018).
1106 53. Lee, Y., Park, J., Park, S.-H. & Shin, E.-C.
1107 CD39⁺CD8⁺ T cells
1108 exhibit a distinct phenotype among tumor-infiltrating tumor-
1109 antigenspecific CD8⁺ T cells. *J. Immunol.* (2019).
1110 54. Blank, C. U. *et al.* Defining 'T cell exhaustion'. *Nat. Rev. Immunol.*
1111 (2019) doi:10.1038/s41577-019-0221-9.
1112 55. McLane, L. M., Abdel-Hakeem, M. S. & Wherry, E. J. CD8 T Cell
1113 Exhaustion During Chronic Viral Infection and Cancer. *Annu. Rev.*
1114 *Immunol.* (2019) doi:10.1146/annurev-immunol-041015-055318.
1115 56. Egelston, C. A. *et al.* Human breast tumor-infiltrating CD8+ T cells retain
1116 polyfunctionality despite PD-1 expression. *Nat. Commun.* (2018)
1117 doi:10.1038/s41467-018-06653-9.
1118 57. Spitzer, M. H. *et al.* Systemic Immunity Is Required for Effective Cancer
1119 Immunotherapy. *Cell* (2017) doi:10.1016/j.cell.2016.12.022.
1120 58. Menares, E. *et al.* Tissue-resident memory CD8+ T cells amplify anti-
1121 tumor immunity by triggering antigen spreading through dendritic cells.
1122 *Nat. Commun.* (2019) doi:10.1038/s41467-019-12319-x.
1123 59. Goddard, E. T., Bozic, I., Riddell, S. R. & Ghajar, C. M. Dormant tumour
1124 cells, their niches and the influence of immunity. *Nature Cell Biology*

1125 (2018) doi:10.1038/s41556-018-0214-0.
1126 60. Aguirre-Ghiso, J. A. Models, mechanisms and clinical evidence for
1127 cancer dormancy. *Nature Reviews Cancer* (2007) doi:10.1038/nrc2256.
1128 61. Koebel, C. M. *et al.* Adaptive immunity maintains occult cancer in an
1129 equilibrium state. *Nature* **450**, 903–907 (2007).
1130 62. Kim, S. Y. *et al.* Role of the IL-6-JAK1-STAT3-Oct-4 pathway in the
1131 conversion of non-stem cancer cells into cancer stem-like cells. *Cell.*
1132 *Signal.* (2013) doi:10.1016/j.cellsig.2013.01.007.
1133 63. Baccelli, I. *et al.* Identification of a population of blood circulating tumor
1134 cells from breast cancer patients that initiates metastasis in a xenograft
1135 assay. *Nat. Biotechnol.* (2013) doi:10.1038/nbt.2576.
1136 64. Slütter, B. *et al.* Dynamics of influenza-induced lung-resident memory T
1137 cells underlie waning heterosubtypic immunity. *Sci. Immunol.* (2017)
1138 doi:10.1126/sciimmunol.aag2031.
1139 65. Welten, S. P. M., Sandu, I., Baumann, N. S. & Oxenius, A. Memory
1140 CD8 T cell inflation vs tissue-resident memory T cells: Same patrollers,
1141 same controllers? *Immunological Reviews* (2018)
1142 doi:10.1111/imr.12649.
1143 66. Pereira, B. I. *et al.* Senescent cells evade immune clearance via HLA-E-
1144 mediated NK and CD8+ T cell inhibition. *Nat. Commun.* (2019)
1145 doi:10.1038/s41467-019-10335-5.
1146 67. Cox, T. R. *et al.* LOX-mediated collagen crosslinking is responsible for
1147 fibrosis-enhanced metastasis. *Cancer Res.* (2013) doi:10.1158/0008-
1148 5472.CAN-12-2233.

1149 68. Goddard, E. T. *et al.* The rodent liver undergoes weaning-induced
1150 involution and supports breast cancer metastasis. *Cancer Discov.*
1151 (2017) doi:10.1158/2159-8290.CD-16-0822.
1152 69. Quail, D. F. *et al.* Obesity alters the lung myeloid cell landscape to
1153 enhance breast cancer metastasis through IL5 and GM-CSF. *Nat. Cell*
1154 *Biol.* (2017) doi:10.1038/ncb3578.
1155 70. Rachman-Tzemah, C. *et al.* Blocking Surgically Induced Lysyl Oxidase
1156 Activity Reduces the Risk of Lung Metastases. *Cell Rep.* (2017)
1157 doi:10.1016/j.celrep.2017.04.005.
1158 71. O'Reilly, M. S. *et al.* Angiostatin: A novel angiogenesis inhibitor that
1159 mediates the suppression of metastases by a lewis lung carcinoma. *Cell*
1160 (1994) doi:10.1016/0092-8674(94)90200-3.
1161 72. Obradović, M. M. S. *et al.* Glucocorticoids promote breast cancer
1162 metastasis. *Nature* (2019) doi:10.1038/s41586-019-1019-4.
1163 73. Albrengues, J. *et al.* Neutrophil extracellular traps produced during
1164 inflammation awaken dormant cancer cells in mice. *Science (80-.).*
1165 (2018) doi:10.1126/science.aao4227.
1166 74. Brummelman, J. *et al.* Development, application and computational
1167 analysis of high-dimensional fluorescent antibody panels for single-cell
1168 flow cytometry. *Nat. Protoc.* (2019) doi:10.1038/s41596-019-0166-2.
1169 75. Picelli, S. *et al.* Full-length RNA-seq from single cells using Smart-seq2.
1170 *Nat. Protoc.* (2014) doi:10.1038/nprot.2014.006.
1171 76. Reimand, J. *et al.* Pathway enrichment analysis and visualization of
1172 omics data using g:Profiler, GSEA, Cytoscape and EnrichmentMap.

1173 *Nat. Protoc.* (2019) doi:10.1038/s41596-018-0103-9.

1174 77. Siliņa, K., Burkhardt, C., Casanova, R., Solterman, A. & van den Broek,
1175 M. A Quantitative Pathology Approach to Analyze the Development of
1176 Human Cancer-Associated Tertiary Lymphoid Structures. in *Methods in*
1177 *Molecular Biology* (2018). doi:10.1007/978-1-4939-8709-2_5.

1178 78. Goldrath, A. W., Luckey, C. J., Park, R., Benoist, C. & Mathis, D. The
1179 molecular program induced in T cells undergoing homeostatic
1180 proliferation. *Proc. Natl. Acad. Sci. U. S. A.* (2004)
1181 doi:10.1073/pnas.0407417101.

1182

Figure 1

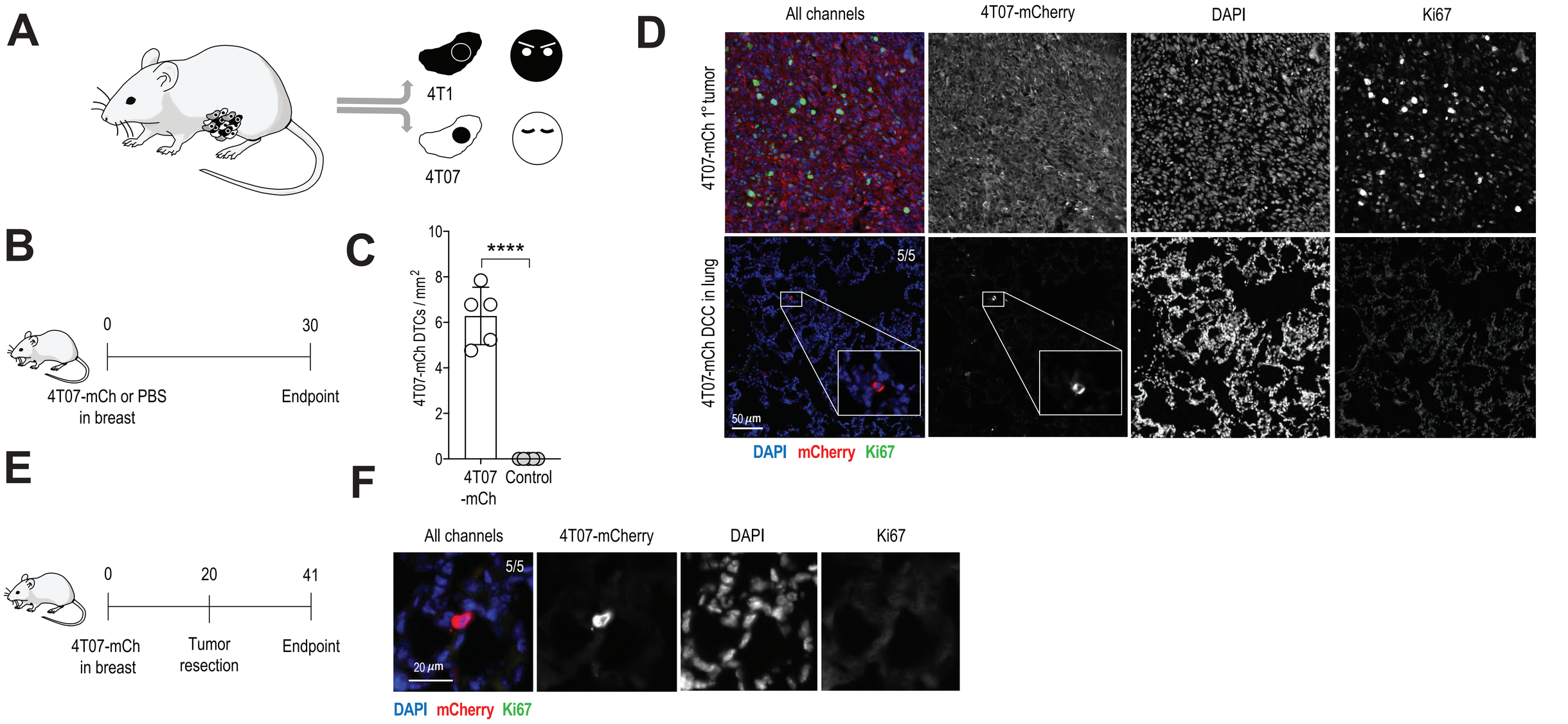
A
4T1
4T07
B
0
30
4T07-mCh or PBS
in breast
Endpoint
C
****
4T07-mCh DTCs / mm2
10
8
6
4
2
0
4T07
-mCh
Control
D
All channels
4T07-mCherry
DAPI
Ki67
4T07-mCh 1° tumor
4T07-mCh DCC in lung
5/5
50 μm
DAPI mCherry Ki67
E
0
20
41
4T07-mCh
in breast
Tumor
resection
Endpoint
F
All channels
4T07-mCherry
DAPI
Ki67
5/5
20 μm
DAPI mCherry Ki67

Figure 2

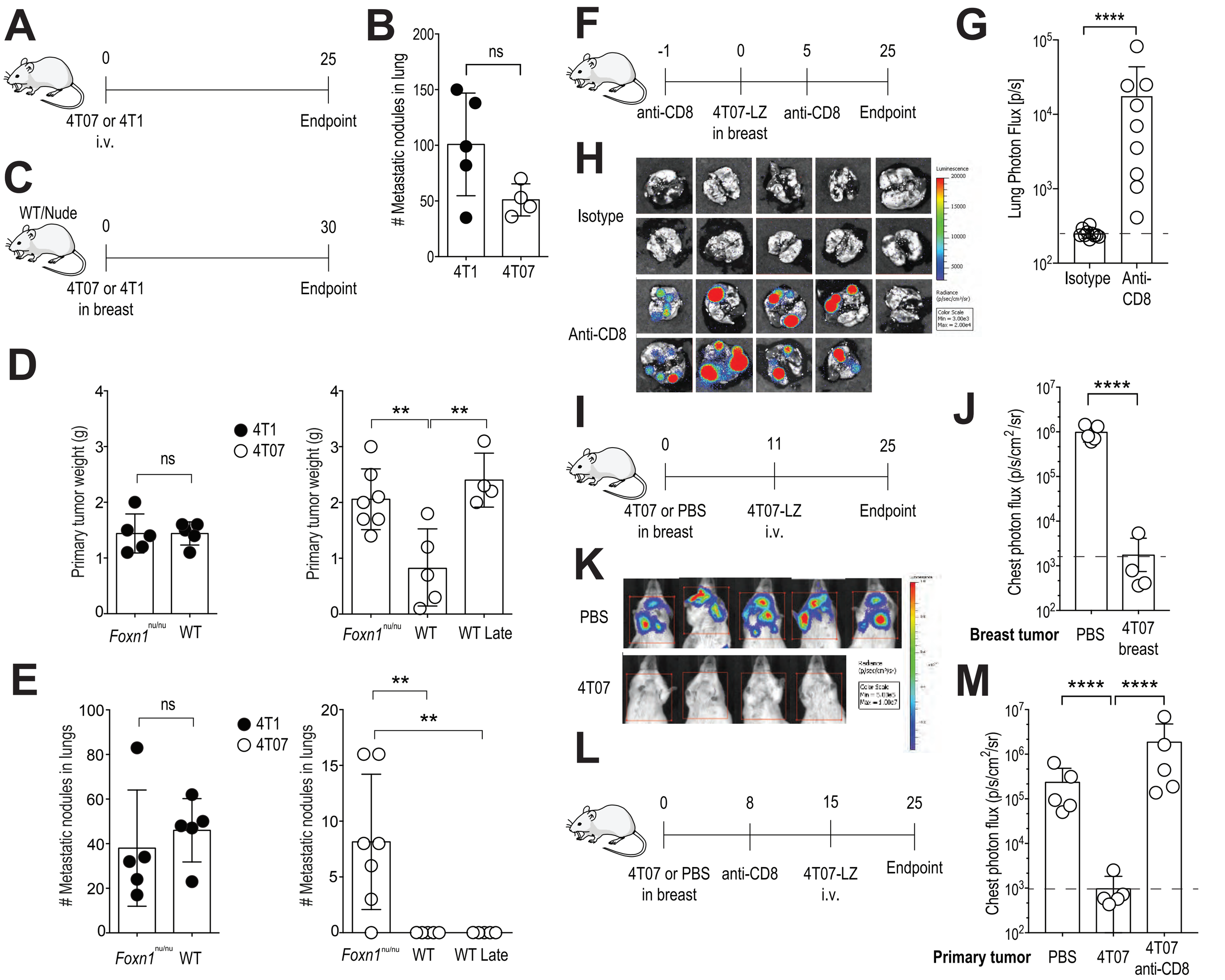
A
0
25
4T07 or 4T1
i.v.
Endpoint
B
ns
Metastatic nodules in lung
4T1
4T07
C
WT/Nude
0
30
4T07 or 4T1
in breast
Endpoint
D
ns
Primary tumor weight (g)
4T1
4T07
Foxn1nu/nu
WT
**
**
WT Late
E
ns
Metastatic nodules in lungs
**
**
F
-1
0
5
25
anti-CD8
4T07-LZ
in breast
anti-CD8
Endpoint
G
****
Lung Photon Flux [p/s]
Isotype
Anti-CD8
H
Isotype
Anti-CD8
Luminescence
Radiance (p/sec/cm²/sr)
Color Scale
Min = 3.00e3
Max = 2.00e4
I
0
11
25
4T07 or PBS
in breast
4T07-LZ
i.v.
Endpoint
J
****
Chest photon flux (p/s/cm²/sr)
Breast tumor
PBS
4T07
breast
K
PBS
4T07
L
0
8
15
25
4T07 or PBS
in breast
anti-CD8
4T07-LZ
i.v.
Endpoint
M
****
****
Chest photon flux (p/s/cm²/sr)
Primary tumor
PBS
4T07
4T07
anti-CD8

Figure 3

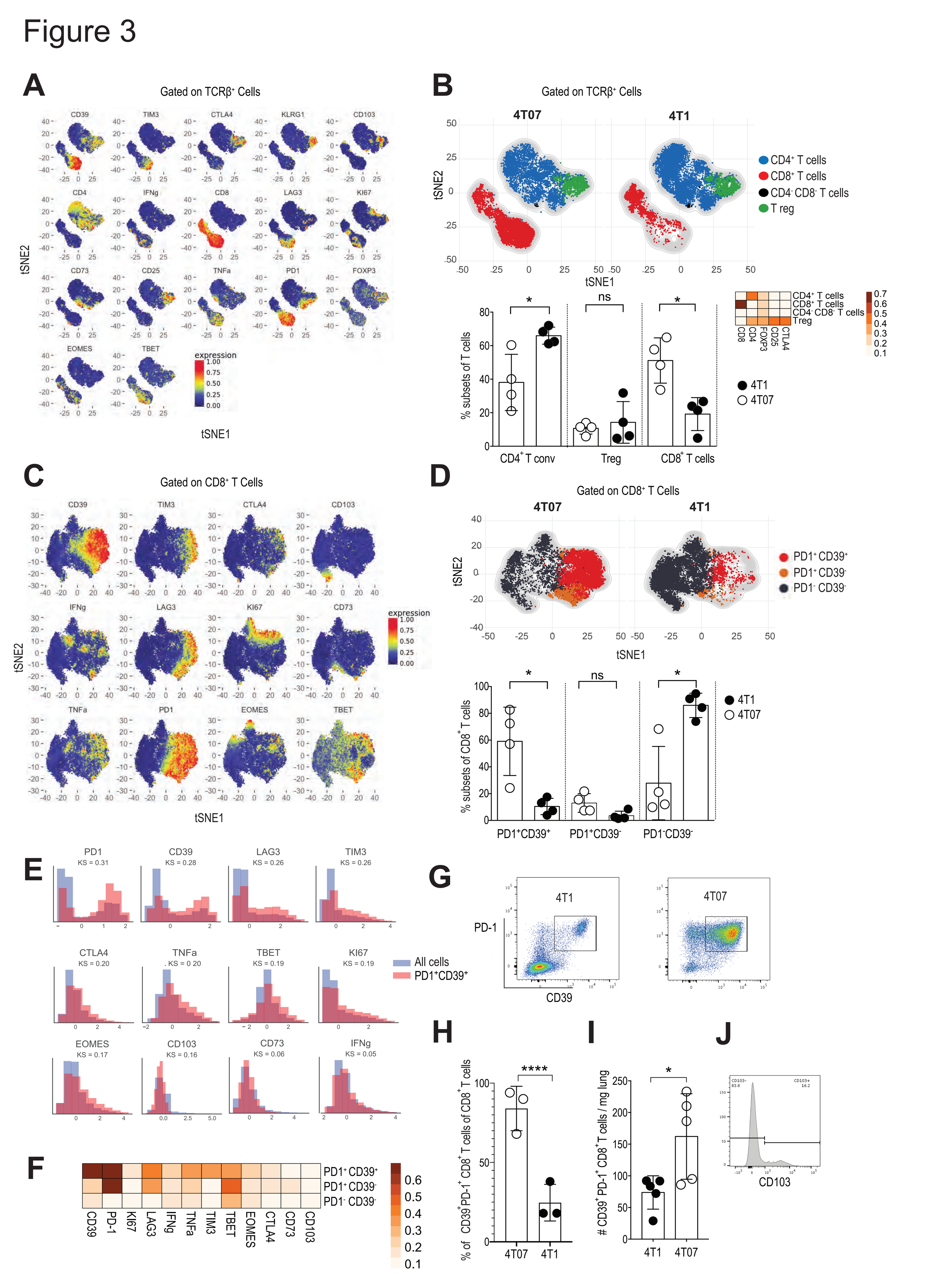
A
Gated on TCRβ+ Cells
CD39
TIM3
CTLA4
KLRG1
CD103
CD4
IFNg
CD8
LAG3
KI67
CD73
CD25
TNFa
PD1
FOXP3
EOMES
TBET
expression
1.00
0.75
0.50
0.25
0.00
tSNE2
tSNE1
B
Gated on TCRβ+ Cells
4T07
4T1
CD4+ T cells
CD8+ T cells
CD4- CD8- T cells
T reg
tSNE2
tSNE1
% subsets of T cells
CD4+ T conv
Treg
CD8+ T cells
ns
*
CD4+ T cells
CD8+ T cells
CD4- CD8- T cells
Treg
CD8
CD4
FOXP3
CD25
CTLA4
4T1
4T07
C
Gated on CD8+ T Cells
CD39
TIM3
CTLA4
CD103
IFNg
LAG3
KI67
CD73
TNFa
PD1
EOMES
TBET
expression
1.00
0.75
0.50
0.25
0.00
tSNE2
tSNE1
D
Gated on CD8+ T Cells
4T07
4T1
PD1+ CD39+
PD1+ CD39-
PD1- CD39-
tSNE2
tSNE1
% subsets of CD8+ T cells
PD1+CD39+
PD1+CD39-
PD1-CD39-
ns
*
4T1
4T07
E
PD1
KS = 0.31
CD39
KS = 0.28
LAG3
KS = 0.26
TIM3
KS = 0.26
CTLA4
KS = 0.20
TNFa
KS = 0 20
TBET
KS = 0.19
KI67
KS = 0.19
EOMES
KS = 0.17
CD103
KS = 0.16
CD73
KS = 0.06
IFNg
KS = 0.05
All cells
PD1+CD39+
G
4T1
4T07
PD-1
CD39
H
% of CD39+PD-1+ CD8+ T cells of CD8+ T cells
****
4T07
4T1
I
CD39+ PD-1+ CD8+ T cells / mg lung
*
4T1
4T07
J
CD103
F
PD1+ CD39+
PD1+ CD39-
PD1- CD39-
CD39
PD-1
KI67
LAG3
IFNg
TNFa
TIM3
TBET
EOMES
CTLA4
CD73
CD103

Figure 4

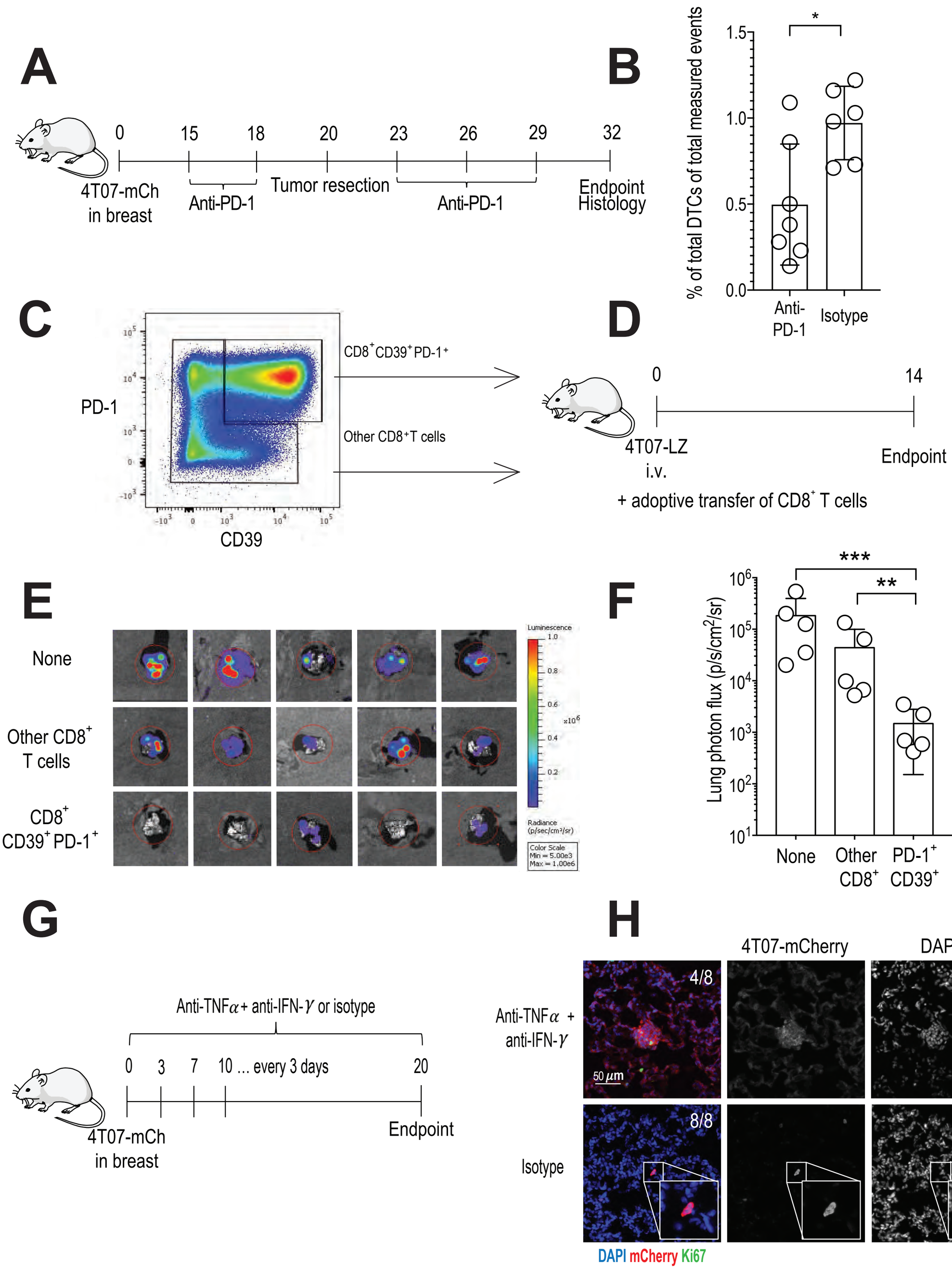
A
0
15
18
20
23
26
29
32
4T07-mCh
in breast
Anti-PD-1
Tumor resection
Anti-PD-1
Endpoint
Histology
B
% of total DTCs of total measured events
1.5
1.0
0.5
0.0
*
Anti-
PD-1
Isotype
C
PD-1
CD39
CD8+CD39+PD-1+
Other CD8+T cells
D
0
14
4T07-LZ
i.v.
Endpoint
+ adoptive transfer of CD8+ T cells
E
None
Other CD8+
T cells
CD8+
CD39+ PD-1+
Luminescence
Radiance
(p/sec/cm²/sr)
Color Scale
Min = 5.00e3
Max = 1.00e6
F
Lung photon flux (p/s/cm²/sr)
***
**
None
Other
CD8+
PD-1+
CD39+
G
Anti-TNFα+ anti-IFN-γ or isotype
0
3
7
10 ... every 3 days
20
4T07-mCh
in breast
Endpoint
H
4T07-mCherry
DAPI
Ki67
Anti-TNFα +
anti-IFN-γ
4/8
50 μm
Isotype
8/8
DAPI mCherry Ki67

Figure 5

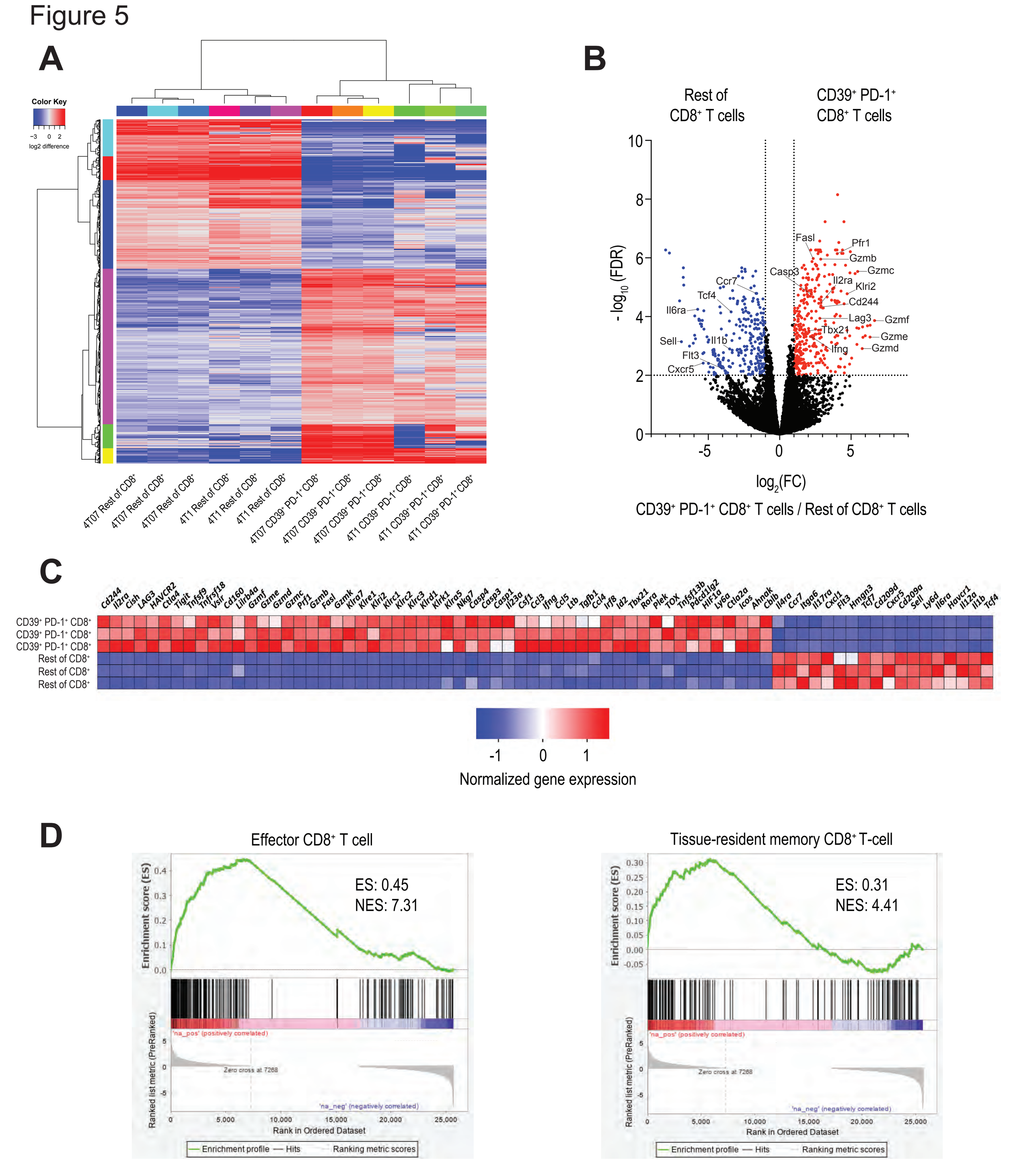
A
Color Key
−3 0 2
log2 difference
4T07 Rest of CD8+
4T07 Rest of CD8+
4T07 Rest of CD8+
4T1 Rest of CD8+
4T1 Rest of CD8+
4T1 Rest of CD8+
4T07 CD39+ PD-1+ CD8+
4T07 CD39+ PD-1+ CD8+
4T07 CD39+ PD-1+ CD8+
4T1 CD39+ PD-1+ CD8+
4T1 CD39+ PD-1+ CD8+
4T1 CD39+ PD-1+ CD8+
B
Rest of CD8+ T cells
CD39+ PD-1+ CD8+ T cells
- log10 (FDR)
log2(FC)
CD39+ PD-1+ CD8+ T cells / Rest of CD8+ T cells
Fasl
Pfr1
Gzmb
Gzmc
Casp3
Il2ra
Klri2
Cd244
Lag3
Gzmf
Tbx21
Gzme
Ifng
Gzmd
Ccr7
Tcf4
Il6ra
Sell
Il1b
Flt3
Cxcr5
C
CD39+ PD-1+ CD8+
Rest of CD8+
Normalized gene expression
D
Effector CD8+ T cell
Tissue-resident memory CD8+ T-cell
ES: 0.45
NES: 7.31
ES: 0.31
NES: 4.41
Enrichment score (ES)
Ranked list metric (PreRanked)
'na_pos' (positively correlated)
'na_neg' (negatively correlated)
Zero cross at 7268
Rank in Ordered Dataset
Enrichment profile
Hits
Ranking metric scores

Figure 6

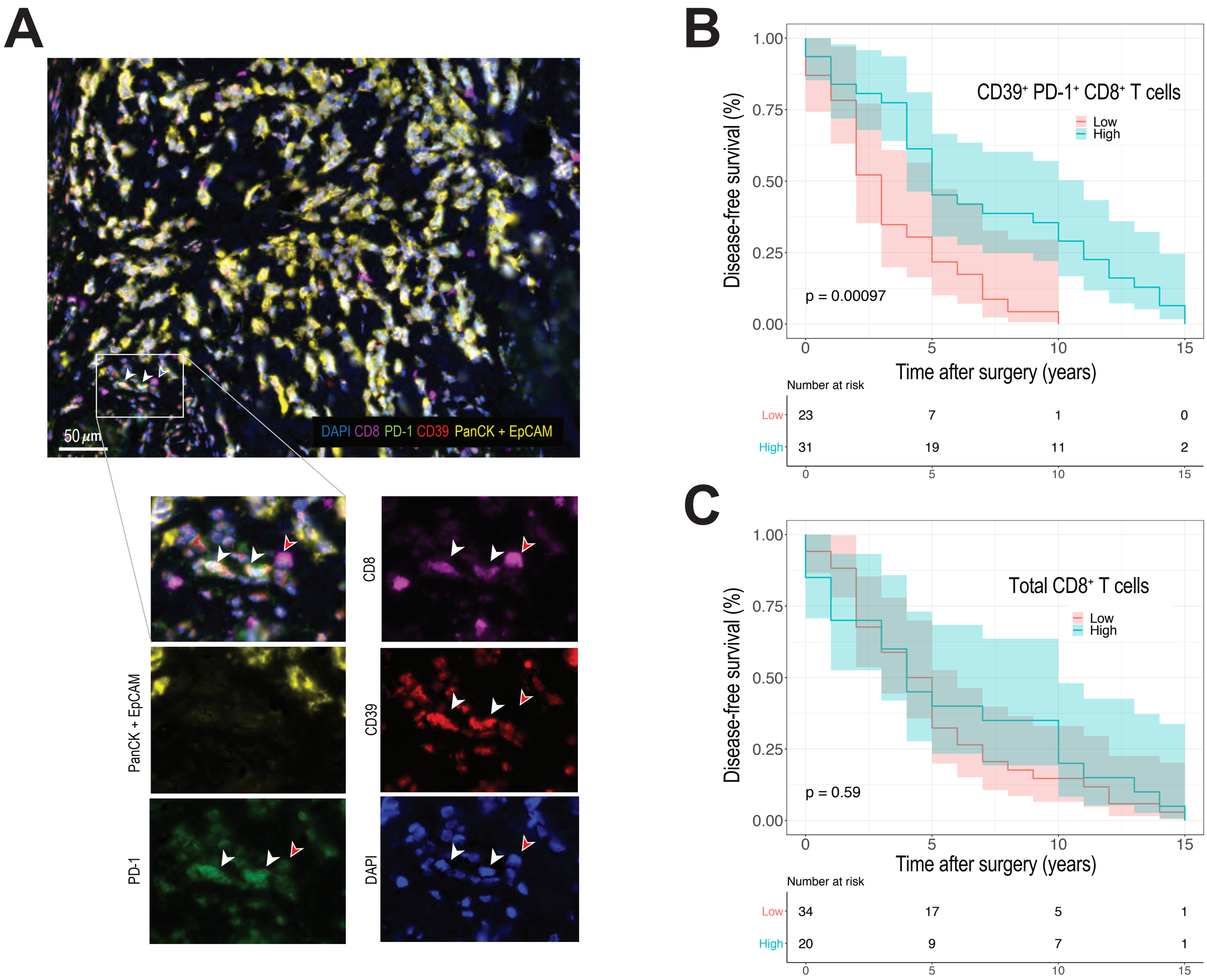
A
50 μm
DAPI CD8 PD-1 CD39 PanCK + EpCAM
PanCK + EpCAM
CD8
PD-1
CD39
DAPI
B
CD39+ PD-1+ CD8+ T cells
Low
High
p = 0.00097
Disease-free survival (%)
1.00
0.75
0.50
0.25
0.00
0
5
10
15
Time after surgery (years)
Number at risk
Low 23 7 1 0
High 31 19 11 2
C
Total CD8+ T cells
Low
High
p = 0.59
Disease-free survival (%)
1.00
0.75
0.50
0.25
0.00
0
5
10
15
Time after surgery (years)
Number at risk
Low 34 17 5 1
High 20 9 7 1